Trade-Offs Between 1-D and 2-D Regional River Hydrodynamic Models

A. Fleischmann, R. Paiva, W. Collischonn, V. A Siqueira, A. Paris, D. Moreira, F. Papa, Al Bitar Ahmad, Marie Parrens, F. Aires, et al.

Water Resources Research

RESEARCH ARTICLE
10.1029/2019WR026812

Trade-Offs Between 1-D and 2-D Regional River Hydrodynamic Models

A. S. Fleischmann[1], R. C. D. Paiva[1], W. Collischonn[1], V. A. Siqueira[1], A. Paris[2], D. M. Moreira[3], F. Papa[4,5], A. A. Bitar[6], M. Parrens[6,7], F. Aires[8], and P. A. Garambois[9]

[1]Hydraulic Research Institute (IPH), Federal University of Rio Grande do Sul (UFRGS), Porto Alegre, Brazil, [2]Collecte Localisation Satellites (CLS), Ramonville Saint Agne, France, [3]CPRM, Rio de Janeiro, Brazil, [4]Universidade de Brasília (UnB), IRD, Institute of Geoscience, Brasilia, Brazil, [5]Université de Toulouse, LEGOS (IRD, CNRS, CNES, UPS), Toulouse, France, [6]CESBIO (CNRS, IRD, CNES, UPS), Toulouse, France, [7]Dynafor, Université de Toulouse, INRAE, INPT, INP-PURPAN, Castanet-Tolosan, France, [8]Sorbonne Université, Observatoire de Paris, Université PSL, Estellus, Paris, France, [9]Irstea, Aix-Marseille University, Aix-en-Provence, France

Key Points:
- We develop a 2-D regional-scale coupled hydrologic-hydrodynamic model in the light of multisatellite visibility
- 2-D model better represents complex wetlands but provides similar results to 1-D on discharge and water levels for large river networks
- Dimensionality is more important than coupling hydrological-hydrodynamic processes to represent the hydraulics of complex tropical wetlands

Supporting Information:
- Supporting Information S1

Correspondence to:
A. S. Fleischmann,
ayan.fleischmann@gmail.com

Citation:
Fleischmann, A. S., Paiva, R. C. D., Collischonn, W., Siqueira, V. A., Paris, A., Moreira, D. M., et al. (2020). Trade-offs between 1-D and 2-D regional river hydrodynamic models. *Water Resources Research*, *56*, e2019WR026812. https://doi.org/10.1029/2019WR026812

Received 22 NOV 2019
Accepted 11 JUN 2020
Accepted article online 14 JUN 2020

Abstract Recent years have seen the development of 1-D and 2-D regional-scale hydrological-hydrodynamic models, which differ greatly from reach-scale applications in terms of subgrid assumptions, parameterization, and applied resolution. Although 1-D and 2-D comparisons have already been performed at reach and local scales, model differences at regional scale are poorly understood. Moreover, there is a need to improve the coupling between hydrological and hydrodynamic models. It is addressed here by applying the MGB model at 1-D and 2-D dimensions for the whole ~700,000 km^2 Negro basin (Amazon), which presents different wetland types. Long-term continuous simulations are performed and validated with multisatellite observations of hydraulic variables. Results showed that both approaches are similarly able to estimate discharges and water levels along main rivers, especially considering parameter uncertainties, but differ in terms of flood extent and volume and water levels in complex wetlands. In these latter, the diffuse flow and drainage patterns were more realistically represented by the 2-D scheme, as well as wetland connectivity across the basin. The 2-D model led to higher drainage basinwide, while the 1-D model was more sensitive to hydrodynamic parameters for discharge and flood extent and had a similar sensitivity for water levels. Finally, tests on the coupling between hydrologic and hydrodynamic processes suggested that their representation in an online way is less important for tropical wetlands than model dimensionality, which largely impacts water transfer and repartition.

Plain Language Summary Hydrologic-hydrodynamic numerical models are powerful tools for improving water resources and disaster management and for the understanding of hydrological processes. Last years have faced the development of regional-scale applications (i.e., areas between 10^4 to 10^6 km^2), with approaches at both 1-D and 2-D dimensions, that is, by representing surface water transport in either one (along rivers) or two horizontal directions (in order to represent flood propagation in wetlands). In this study, we present a regional-scale application of the MGB model at both 1-D and 2-D dimensions for the Negro River Basin in the Amazon and compare its capability to simulate processes at the basin scale and for different wetland types. We show that current 1-D and 2-D models are similarly capable to represent discharges and water levels along main rivers, but for more complex wetlands, the 2-D models are required, especially for estimating water levels. We also show that for tropical wetlands, the consideration of feedbacks between hydrologic and hydrodynamics is less important than the dimensionality of the model (i.e., if it is 1-D or 2-D). New lessons on the functioning of complex river-wetland systems in the Amazon are presented, in special consideration of the current availability of remote sensing data sets.

1. Introduction

Recent years have seen the development of regional- to global-scale river hydrodynamic models at increasing resolution, using either the full Saint-Venant equation or its simplifications (diffusive and local inertia) and adopting either 1-D or 2-D schemes (Bates et al., 2018; Dottori et al., 2016; Falter et al., 2016; Getirana et al., 2017; Mateo et al., 2017; Paiva et al., 2013; Paiva et al., 2011; Pontes et al., 2017; Sampson et al., 2015; Schumann et al., 2016; Yamazaki et al., 2013; Yamazaki, Sato, et al., 2014). These models are important tools for flood risk assessment (Pappenberger et al., 2012; Trigg et al., 2016; Winsemius et al., 2016), flood

forecasting (Kauffeldt et al., 2016), climate change studies (Hirabayashi et al., 2013; Sorribas et al., 2016), and understanding of biogeochemical cycles and hydrological processes (Getirana et al., 2017; Paiva et al., 2013).

Modeling continental river dynamics faces great challenges such as quantitatively evaluating the implications of upscaling Saint-Venant river models to continental scale and estimating river geometry (Hodges, 2013), and its ultimate goal is to provide locally relevant estimates at hyperresolution (Bierkens et al., 2015; Fleischmann et al., 2019; Wood et al., 2011). Intercomparison projects between global models have showed the necessity of improving routing schemes with hydrodynamic modules (Zhao et al., 2017) and the potentiality of continental 1-D models with floodplain modules to represent large-scale flooding (Trigg et al., 2016). In this latter, however, a case study in the African continent showed relevant discrepancies between models in large deltas and arid/semiarid wetlands (Trigg et al., 2016), which frequently present complex 2-D hydrodynamic flow patterns.

1-D models have often proved satisfactory to represent river processes such as flood wave diffusion, floodplain storage, backwater effects, and river discharges (Paiva et al., 2013; Yamazaki et al., 2011). However, many floodable regions across the globe are subject to a more complex hydrodynamics than what 1-D models can address, since a single upstream-downstream connectivity is not able to represent the floodplain flows subparallel to the main river channel and the complex diffuse flow, connectivity, and multichannel patterns that actually exist (Alsdorf et al., 2007; Altenau et al., 2017; Czuba et al., 2019; Park & Latrubesse, 2017; Pinel et al., 2019; Trigg et al., 2009; Wilson et al., 2007). CaMa-Flood (Yamazaki et al., 2011; Yamazaki, Sato, et al., 2014) and MGB (Pontes et al., 2017) are examples of large-scale 1-D hydrodynamic models that have implemented bifurcation and lateral connection schemes (i.e., connections among multiple neighbor river reaches) to improve the connectivity across floodable areas, trying to move away from a single upstream-downstream flow direction. Indeed, it is generally expected that 2-D (or coupled 1-D/2-D) models should provide a more realistic and coherent framework for representing flood inundation dynamics, in comparison to 1-D large-scale hydrodynamic models with simple storage floodplain units (Neal et al., 2012; Schumann et al., 2016). However, the extension of these differences were not well explored in the literature. Classically hindered by computational limits, 2-D models are now feasible at regional to global scales for both extreme events (Alfieri et al., 2013; Dottori et al., 2016; Sampson et al., 2015; Wing et al., 2017) and continuous simulation (Andreadis et al., 2017; Hoch et al., 2017; Schumann et al., 2016). The advent of new remote sensing missions dedicated to surface hydrology, such as the Surface Water and Ocean Topography (SWOT), also push toward the development of more detailed hydrodynamic models.

Furthermore, while most large-scale hydrologic-hydrodynamic models perform an offline coupling by forcing a hydrodynamic model with outputs from a rainfall-runoff model (Biancamaria et al., 2009; Getirana, Kumar, et al., 2017; Grimaldi et al., 2019; Hoch et al., 2017; Mejia & Reed, 2011) or with observed discharges (Sampson et al., 2015; Schumann et al., 2016), current efforts are aiming to perform strong (two-way) coupling with feedbacks between the hydrological and hydrodynamic modules. Examples include the applications by Da Paz et al. (2014) in the Pantanal and Fleischmann et al. (2018) in the semiarid Niger Inner Delta. In the latter case, the modeling framework represented both the dynamic evapotranspiration in flooded areas and infiltration from flooded areas into the unsaturated soil column. The extent to which these coupling strategies may be relevant for tropical wetlands is still unknown.

The extent to which 2-D regional-scale models are preferable from 1-D ones, and for which purposes or variables of interest, remains an open question. If 2-D hydrologic-hydrodynamic models at the regional scale are now feasible due to increasing remote sensing data sets and computational power, should we favor it to the detriment of the 1-D approach? One important step then is to understand how much detail 1-D models miss in comparison to 2-D ones with dynamic floodplain fluxes, in terms of changes in relevant hydrodynamic variables or missing hydrodynamic process representation, and to which extent the high uncertainty in 2-D model parameterization reduced the benefit of increased dimensionality. Although comparisons between 1-D and 2-D hydraulic models have already been carried out in the literature for the reach scale and often for urban areas (Alho & Aaltonen, 2008; Chatterjee et al., 2008; Cook & Merwade, 2009; Dimitriadis et al., 2016; Horritt & Bates, 2002), this is not the case for regional-scale models, which differ from the reach scale ones in terms of applied resolution, parameterizations, and subgrid assumptions. Such assessments also require intense validation procedures, considering not only water levels and discharges at few observation locations in main rivers but also basinwide distributed information of water

levels (at-a-station and longitudinal profiles) and flood extent (Fleischmann et al., 2019). Of special interest, regional model validation of the dynamics of wetlands (connected or not to adjacent rivers) need to be better addressed, and this is now possible under the satellite era with multiple remote sensing-derived products.

In this context, three main goals are defined for this study: first, to develop and evaluate a 2-D hydrologic-hydrodynamic model with a two-way coupling scheme for regional-scale applications, where the 2-D scheme is applied to the whole basin domain and not only to flood-prone areas; second, to assess the importance of the 2-D scheme in comparison to a 1-D one, in terms of processes representation and impacts on important hydrodynamic and hydrological variables such as discharge, water level, and flood extent and volume. For this, a thorough model validation is performed with multiple in situ and remote sensing products at the regional scale (flood extent, water levels, and water surface slope). Finally, we aim to evaluate the importance of the two-way coupling between hydrology and hydrodynamics in the 2-D and 1-D approaches. We believe that our discussion will provide new insights on the direction of regional- to continental-scale modeling, especially for the simulation of basins with complex wetlands.

2. Material and Methods

2.1. MGB Model

2.1.1. Model Overview

MGB is a semidistributed rainfall-runoff model developed for large-scale basins (Collischonn et al., 2007; Pontes et al., 2017). The basin is divided into unit-catchments using a fixed-length, vector-based discretization (Siqueira et al., 2018), which in turn are divided into hydrologic response units (HRUs) where vertical hydrological processes as canopy interception, evapotranspiration, and soil infiltration are considered to model the generation of surface, subsurface, and groundwater flows. Each unit-catchment is forced with observed precipitation and climate data, which are interpolated to the corresponding centroid. The calculated flux is routed within three linear reservoirs (surface, subsurface, and groundwater). The inertial flood wave routing method (Bates et al., 2010; Neal et al., 2012) is then employed for propagating flows along the drainage network. Evapotranspiration (i.e., soil/vegetation evapotranspiration and open water evaporation) is dynamically computed considering the cell flood fraction at each time step. The 1-D hydrodynamic model version considers floodplains as storage units, where the main channel and floodplain have the same water level, and river-floodplain flow exchange is proportional to the floodplain flooded area at a given water level (Paiva et al., 2011). Its potential drawbacks are related to the expected low capabilities of 1-D models to represent complex or 2-D flow patterns. For more details and equations on both rainfall-runoff modeling and 1-D routing approaches, see the Supplementary Material S1 in Siqueira et al. (2018).

2.1.2. 2-D Scheme for Surface Hydrodynamics

A 2-D (or quasi-2-D) hydrodynamic propagation method was adapted and implemented into the MGB model framework, enhancing the current version by incorporating fluxes in the two horizontal directions and by separately computing floodplain and channelized flows. Within the 2-D scheme, the basin is discretized into a cell grid instead of unit-catchments (Figure 1). A subgrid method is applied, where a high-resolution digital elevation model (DEM) is used to derive subgrid information for the coarse-resolution cells. A cell is defined as the coarse-resolution grid element (i.e., the model calculation unit or model resolution) and a pixel as the high-resolution DEM grid element, following literature (see Figure 2 in Paz et al. (2006) for a clear definition). For a given cell, floodplain flow is calculated for its D4 faces (i.e., orthogonal cell neighbors), while channel flow is computed between a cell and all its D8 neighbors that contain channels. The adopted conceptualization is based on the LISFLOOD-FP subgrid model developed by Neal et al. (2012), while integrating new features such as the consideration of local runoff generation within each cell in a coupled hydrologic-hydrodynamic strategy, that is, by allowing feedbacks between flooded areas and the adjacent soils, and by dynamically representing evapotranspiration in the flooded/nonflooded soil surfaces. Also, floodplain topography is derived from a high-resolution DEM, instead of considering a two-stage compound channel. A drainage network is derived from DEM processing and a predefined area threshold (i.e., a number of pixels that defines the beginning of drainage) upon a flow accumulation map, following the algorithms proposed by Siqueira et al. (2016), and the channel cross section is considered as rectangular based on bankfull width and depth parameters.

At each time step, the ith cell storage (continuity equation; Equation 1) is updated with the respective flows (see Equation 2) and local runoff (hydrological module):

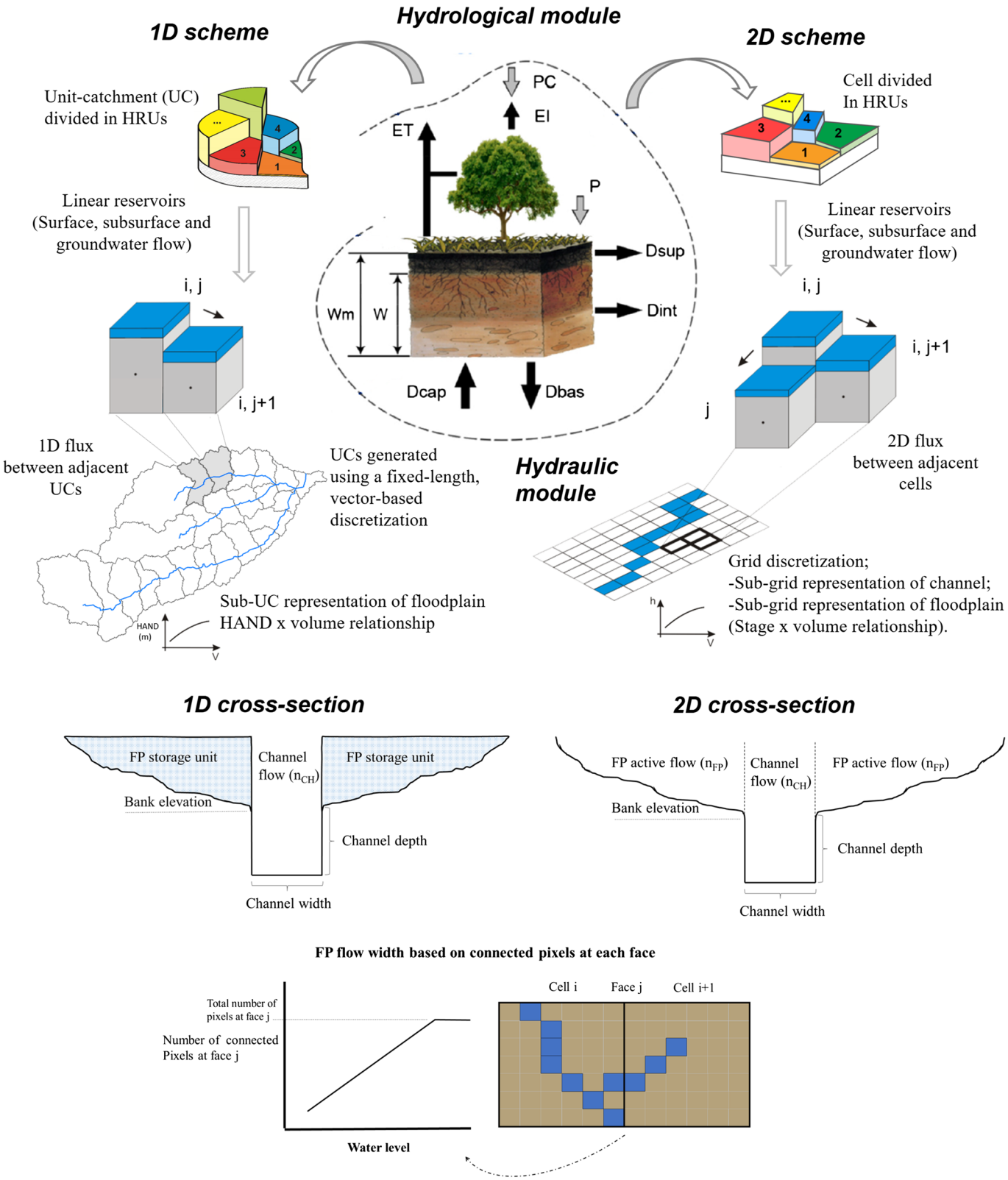

Figure 1. General representation of the MGB model for 1-D and 2-D schemes, with the distinction between hydrological and hydraulic (or hydrodynamic) modules and the coupling between them. The adopted scheme for cross sections for 1-D and 2-D models are depicted, together with the 2-D conceptualization for floodplain (FP) flow depth and width.

$$\frac{V_i^{t+\Delta t} - V_i^t}{\Delta t} = \sum_{j=1}^{nCh} Q_{ch,j}^{t+\Delta t} - \sum_{j=1}^{nFP} Q_{fp,j}^{t+\Delta t} + Q_{cell,i}^{t+\Delta t} - E_{f,i}{}^t + P_{f,i}{}^t - Inf_{f,i}{}^t \quad (1)$$

where *ch* stands for channel, *fp* for floodplain, *cell* for cell, and *f* for flooded areas. $V_i^{t+\Delta t}$ is the stored volume in cell i in time $t + \Delta t$, Δt the time step, $Q_{ch,j}^{t+\Delta t}$ the channel flows for each of the *nCh* channel cell faces, $Q_{fp,j}^{t+\Delta t}$ the floodplain flows for each of the *nFP* floodplain cell faces, $Q_{cell,i}^{t+\Delta t}$ the local runoff at cell i, $E_{f,i}{}^t$ and $P_{f,i}{}^t$ the evaporation and precipitation over flooded areas, respectively, and $Inf_{f,i}{}^t$ the infiltration from flooded areas into soils. The local runoff is computed by the rainfall-runoff module, which estimates the generated runoff within a given cell at each time step based on vertical hydrological processes (canopy interception, evapotranspiration, and soil infiltration) and hillslope routing. The local runoff is affected by the hydraulic model in the adopted online coupling strategy, as described below in "Online coupling."

From the updated storage, the cell water level is obtained from the storage-level relationship derived from DEM processing (Paiva et al., 2011; Yamazaki et al., 2011). This relationship is obtained in a preprocessing step by considering the incremental storage for each increment of stage (trapezium integration). Although it is a commonly adopted approach in 1-D models, large-scale 2-D models as LISFLOOD-FP have been considering two-stage channels for each cell, where flow is either confined to the main channel (with predefined channel width and bankfull depth) or to the second stage floodplain (with width computed as the whole cell size) (Neal et al., 2012).

The model topology for channel-floodplain interactions is based on predefined pair lists of neighbor floodplain and channel cells. For each time step, channel and floodplain fluxes between neighbor cells are decoupled from each other, that is, the coupling is performed through the mass balance in Equation 1 by accounting for various lateral fluxes on a cell. Then, they are computed separately in an explicit scheme at the connecting face j with the dynamic equation developed by Bates et al. (2010):

$$Q_j^{t+\Delta t} = \frac{Q_j^t - g b_j \Delta t \mathrm{h}_j^t \mathrm{S}_j^t}{1 + \frac{g \Delta t \left(\left|Q_j^t\right|\right) n_j{}^2}{b_j \left(\mathrm{h}_j^t\right)^{7/3}}} \quad (2)$$

where $Q_j^{t+\Delta t}$ is the flow calculated at connection j (floodplain or channel) at time step $t + \Delta t$, g the gravitational acceleration, b the flow width, h the flow depth, S the water surface slope, and n the Manning friction coefficient (for floodplain or channel).

The next paragraphs describe each term of Equation 2.

Flow depth (*h in Equation 2*). For a given cell, flow depth is computed as

$$h_t = \max\left(y_i^t, y_{i+1}^t\right) - \max\left(z_i^t, z_{i+1}^t\right) \quad (3)$$

where $y_{i,t}$ is the water surface elevation at cell i and time step t, and z_i^t the floodplain or channel bottom (or bed) elevation. y_i^t is obtained from the DEM-derived stage-volume relationship, and z is constant for channels and level-dependent for floodplains flows.

For channelized flow, the bottom elevation z is obtained from the bank elevation (z_{ref}) subtracted by the channel bankfull depth (h_{bf}). z_{ref} is defined as the average of high-resolution DEM pixels located above the drainage network within the cell. The raw (original) DEM is used to estimate z_{ref}, since a hydrologically conditioned DEM (e.g., after correction from pit filling/removal methods) may have unrealistic elevations. The drainage network is obtained from geoprocessing with the IPH-HydroTools package. h_{bf} may be obtained from in situ observations or simplified geomorphic relationships (see next section for the data used in this study). The main channel cross section is assumed to be rectangular.

For floodplain flow, z is calculated within a cell for each time step as the difference between water surface elevation (y) and the average floodplain water depth ($h_{m,FP}$), where $h_{m,FP}$ is computed as the ratio between floodplain volume and floodplain flooded area. This means that the floodplain average bottom elevation for

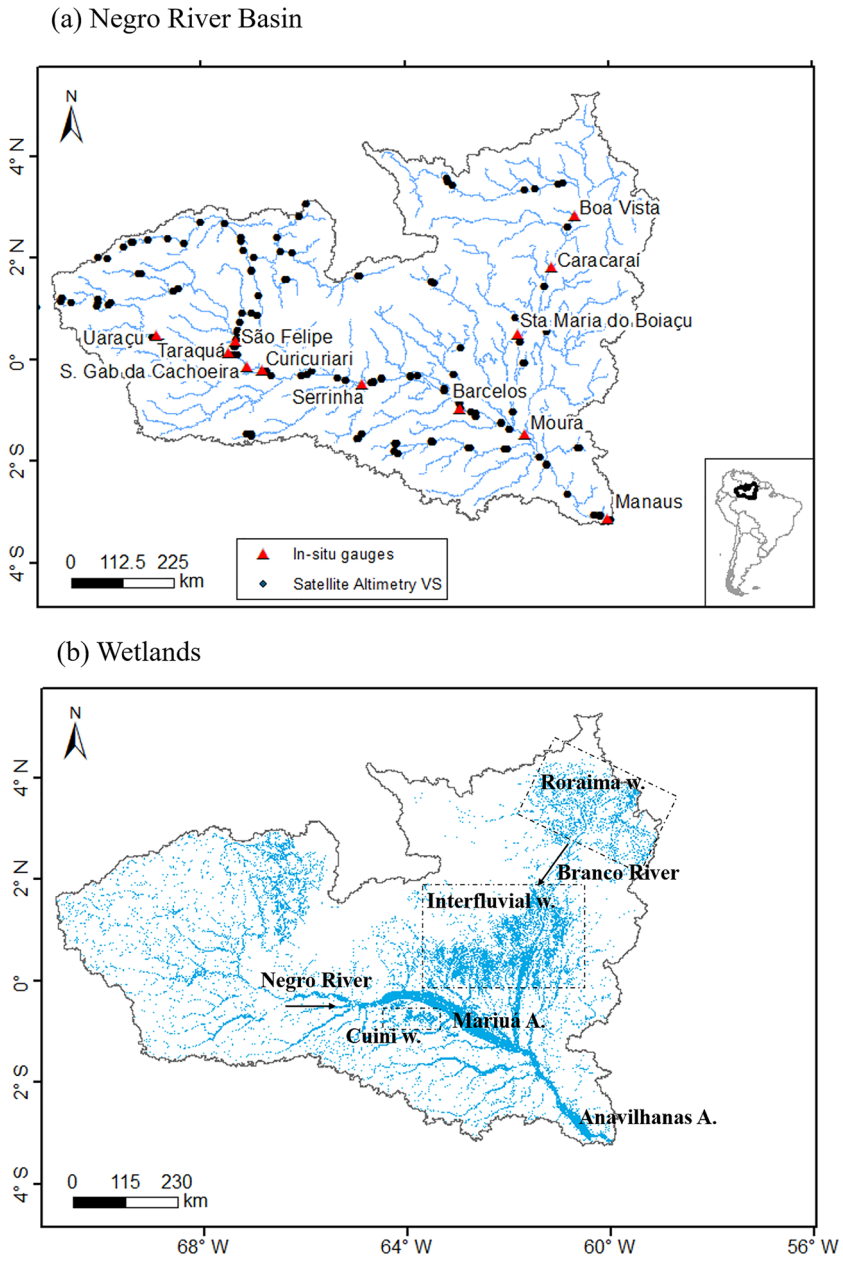

Figure 2. (a) Negro River Basin with in situ water level gauges and satellite altimetry virtual stations (VS). (b) Main wetlands in the basin with regions of interest mentioned in the text: Roraima, interfluvial (in the context of this study only; elsewhere the Roraima and Cuini are also considered interfluvial wetlands) and Cuini wetlands, and Mariuá and Anavilhanas archipelagos. Arrows indicate the preferential flow direction of Negro and Branco Rivers.

a given cell is level-dependent, that is, it depends on how much of the floodplain is flooded. The higher is the flood level, the higher will be the average floodplain bed elevation. For each time step, z is assumed the same for all cell faces.

Flow width (*b in Equation 2*). For a given pair of neighbor cells, channel flow width is estimated as the average bankfull width of the two connected cells, which are typically obtained with hydraulic geometry relationships (i.e., simplified relationships using predictive variables as upstream drainage area or average discharge, which are then applied to each river reach) or satellite data (Allen & Pavelsky, 2018; Frasson et al., 2019; Yamazaki, O'Loughlin, et al., 2014).

Floodplain flow width is computed by counting, for each cell face and for a given water level, the number of pixels that are connected at both faces. When the whole face is connected, the cell size is adopted as the flow width (Figure 1).

Water surface slope (*S in Equation 2*). Water surface slope is computed for both channel and floodplain flows as the difference between water levels in neighbor cells divided by a length. The latter is defined as the cell size for orthogonal fluxes (i.e., between the cell and its orthogonal neighbors) and as the cell diagonal length for fluxes between neighbors in the diagonal direction.

Time step and flow limiter. Time step (Δt) is calculated following the Courant condition with an additional alpha parameter ($\propto$) for ensuring model stability (Bates et al., 2010; Yamazaki et al., 2011):

$$\Delta t = \propto \frac{\Delta x}{\sqrt{gh}} \tag{4}$$

where Δx is the cell length. To further enhance stability, a simple flow limiter was adopted to avoid supercritical regime. This was carried out by constraining velocity at each face so that the Froude number does not exceed unity:

$$Q_j^t = \min\left(Q_j^t, bh^{1.5}g^{0.5}\right) \tag{5}$$

This criterion was sufficient to avoid mass balance errors basinwide and in practice was only applied for very steep upstream reaches, leading to very small differences in downstream reaches.

Online coupling. Finally, a tight coupling strategy is performed through online coupling between hydrologic and hydraulic modules. For each cell within the basin domain, infiltration from flooded areas into the variably saturated soil column ($Inf_{f,i}$ in Equation 1) is considered following the approach by Fleischmann et al. (2018), where the infiltration rate is proportional to the soil dryness. In addition, evapotranspiration is dynamically computed considering the cell flooded fraction at each time step (as defined by Equation 4) as the surface area available for open water evaporation with Penman equation and evapotranspiration in the remaining nonflooded area with Penman-Monteith equation.

2.2. Case Study: Negro River Basin, Amazon

Given its large dimensions and the varied wetland types associated to it, the Negro River Basin in the Amazon was considered an interesting case study for evaluating regional-scale river hydrodynamic models, especially in terms of their capacity of simulating complex river-wetlands systems. The Negro River (Figure 2) has a drainage area of ~700,000 km^2 and is the second largest tributary of the Amazon River (after the Madeira River). More than 90% of the basin is located within Brazil (Latrubesse & Stevaux, 2015), and its confluence with the Amazon River is located in the city of Manaus. Backwater effects from Amazon mainstem occurs in its downstream 300–400 km reach (Meade et al., 1991). The main tributary is the Branco River, which is the main sediment provider for the basin. The Negro River has also two huge fluvial archipelagoes (Mariuá—between Serrinha and Moura stations; and Anavilhanas, downstream of Moura; see Figure 2), which are associated to anabranching geomorphological patterns with a multichannel system with stable islands (Latrubesse & Stevaux, 2015). The basin has a seasonal precipitation regime with maximum (minimum) at MJJ (DJF) months and average annual rainfall around 2,000–2,200 mm (Latrubesse & Stevaux, 2015). Altitudes range from ~3,000 m highlands in the Pico da Neblina (highest peak in Brazil; 2,995 m) and "tepuis" Precambrian table mountains (e.g., the Monte Roraima) to the lowlands around Manaus city at 92 m.

Wetlands in the basin can be divided into two main groups: river floodplains and interfluvial wetlands, which sum up to 119,600 km^2 of floodable areas (Melack & Hess, 2010) and have a floodplain seasonal storage variation ranging from ~170 km^3 (Frappart et al., 2008) to 331 km^3 (Frappart et al., 2005). Floodplains along the Negro River mainstem and its tributaries are locally known as "igapós." They are acid, black-water river systems and are generally nutrient and sediment poor, presenting small biodiversity in contrast to the sediment-rich, white rivers' floodplains ("várzeas") in the Amazon basin.

Besides river floodplains, the Negro River Basin presents complex and poorly known interfluvial wetlands (Figure 2b), which are very different from the well-studied Central Amazon wetlands (Belger et al., 2011), and were called the "Septentrional Pantanal" by Santos et al. (1993) given their large extension. They occur in flat terrains associated to low density vegetation, called "campinas" (open, herbaceous vegetation) and "campinaranas" (mixed herbaceous-arboreal formation) and present hydromorphic, spodosol sandy soils. Most of them have been recently described as formed by neotectonic events associated to megafan systems (Rossetti et al., 2012). Flooding in these areas are typically related to high water table levels associated with local rainfall and is less dependent of flooding from adjacent large rivers. During the dry period, there can occur water deficit and a deep water table (Guimarães & Bueno, 2016). A detailed description of the Viruá megafan, the most well-studied interfluvial wetland in the Negro basin, is presented in Rossetti et al. (2017). In the Roraima Brazilian state in the basin northeast, wetlands in savanna-like vegetation are also present (the Rupununi wetlands), usually associated to small river floodplains (Hamilton et al., 2002) (Figure 2b).

2.3. Model Application in the Negro River Basin

The MGB model was applied to the Negro River Basin with both 1-D and 2-D schemes. It was run from 1 January 1999 to 31 August 2015 and was forced with daily TMPA 3B42 precipitation (Huffman et al., 2007) and long-term climate averages from CRU database (New et al., 2002) for wind speed, relative humidity, air temperature, and sunlight hours variables, which are used for evapotranspiration computation.

The vegetation-corrected, high-resolution MERIT DEM (Yamazaki et al., 2017) was used to estimate floodplain topography at 250 m resolution, and a low-pass filter was used to filter out noise across the floodplain terrain. Channel bank elevation was derived from the average of DEM pixels above river reaches, following the methodology by Siqueira et al. (2018) and using the IPH-HydroTools GIS toolkit (Siqueira et al., 2016). The same bank elevation values were adopted for both 1-D and 2-D approaches. The stage-area-volume relationships were computed by integrating areas with a level-pool method for the 2-D model (i.e., by horizontally computing the flooded pixels below a given water level). For the 1-D model, it was based on a HAND contour map (Height Above The Nearest Drainage; Rennó et al., 2008), considering the flooded area associated to each height above the bankfull elevation (see a description of this method in Siqueira et al. (2018)).

For the 2-D model, it is necessary to identify cells with channels, which were defined to match the same drainage network as the 1-D model, in order to ensure model comparability. The only exception was made for wetlands areas, since many interfluvial wetlands have predominantly a diffuse flow pattern without a well-defined drainage pattern. Thus, the high-resolution drainage network developed by Seyler et al. (2009) and based on JERS-1 image classification was combined with the flood extent map by Hess et al. (2015) to infer wetland cells without channels (Figure S1d in the supporting information).

Bankfull width (W) was defined with geomorphic relationships with drainage area (A_d), based on an adjustment with in situ surveyed cross sections, while depth values (D) were derived from the regression equation by Paiva et al. (2013), multiplied by a calibration parameter a (assumed constant for the whole basin). Depth values must be calibrated since they have high uncertainties and are difficult to be observed from remote sensing in comparison to other variables as width.

$$W = 0.1419{A_d}^{0.7662}, \text{ for the Negro River} \tag{6}$$

$$W = 0.2568{A_d}^{0.7057}, \text{ for the Branco River} \tag{7}$$

$$D = a1.26{A_d}^{0.20}, \text{ for the whole basin.} \tag{8}$$

The model was manually calibrated considering only two in situ discharge gauges (Serrinha and Caracaraí, see Figure 2a) to avoid model overparameterization; that is, only two rainfall-runoff parameter sets were calibrated for the whole basin. This is important to yield more physically based, parsimonious model parameter sets (Siqueira et al., 2018) in the way that a sufficient (yet small) number of parameter sets were adopted to allow a good representation of the physical processes. The rainfall-runoff module parameters and the a multiplier (Equation 8) were also parsimoniously calibrated. HRUs were used to define homogeneous regions for the rainfall-runoff parameters and were derived from the South America HRU map developed by Fan et al. (2015) and available at <https://www.ufrgs.br/lsh/products/remote-sensing/simplified-hydrological-response-units-map-for-south-america/>.

Figure 1 compares the 1-D and 2-D model configurations. The 2-D model was set with ~4 km spatial resolution (a 4.17 km actual resolution was obtained from an upscaling of 3 arcsec resolution by a factor of 4.5), totaling 39.882 units with area 17.4 km^2, while the 1-D model is based on 24.115 unit-catchments (average area $\pm$ standard deviation equaling 28.8 $\pm$ 11.2 km^2) defined as the local drainage area of 10 km river reaches. In both cases, the basin downstream boundary condition was set as the observed in situ water level at Manaus, the Manning coefficient was globally set to 0.035 for channel and 0.1 for floodplains, and the time step alpha parameter for model stability adopted as $\propto = 0.3$, leading to time step values around a few minutes. Mass conservation was assessed for all model runs.

The 1-D and 2-D models were compared in terms of their capacity to represent hydrodynamic variables (discharge, absolute water level, water level anomaly—i.e., water level minus long term average, and flood extent and volume). The coupling scheme between hydrological and hydrodynamic processes was assessed through simulation tests with and without coupling and its impact on the water balance components (evapotranspiration and runoff). The considered scenarios were "default" (i.e., with open water evaporation and without infiltration), "Inf" (with infiltration from floodplain into soil), and "NoETw" (without flooded areas open water evaporation). To compare time series of models and observations and the 1-D and 2-D model estimates between them, the following performance metrics were calculated: Nash-Sutcliffe coefficient (NSE), Pearson correlation (r), root mean square error (RMSE), relative RMSE (RMSEr—RMSE normalized by the average observation), delay index (DI—time lag in days that leads to maximum cross-correlation between simulation and observation; Paiva et al., 2013), and bias (relative difference between long term averages). Differences between 1-D and 2-D models are reported as RMSD and RMSDr (i.e., root mean square deviation). To compare maximum flood extents, the critical success index (*CSI*) was computed:

$$CSI = 100(A \cap B)/(A \cup B) \tag{9}$$

where A and B are the observed and simulated flood extents for a given area, respectively. *CSI* ranges from 0% to 100%, where 100% is the optimum value.

2.4. Validation Data Sets

Model outputs were validated against independent flood extent and water level data. Flood extent and surface water estimates from Global Inundation Extent from Multi-Satellites-D3 (GIEMS-D3; Aires et al., 2017), Surface WAter Fraction-High Resolution (SWAF-HR; Parrens et al., 2019) and Hess et al. (2015) were used for model validation.

GIEMS-D3 (Aires et al., 2017) is a unique data set that provides high-spatial-resolution (~90 m) inundation extent globally at a monthly time scale over the 1993–2007 period. It relies on the downscaling of GIEMS data set (Prigent et al., 2007, Papa et al., 2010), which is based on the data fusion of multiple satellite observations (passive and active microwave and visible and near-infrared reflectances). This downscaling is performed from the original 25 km resolution to the 90 m resolution through a floodability index model derived from a global topography and hydrology from HydoSHEDS (Lehner et al., 2008). Compared to other global high-resolution data sets based on visible or infrared observations, GIEMS-D3 has the advantage to detect water below the vegetation (Aires et al., 2018). GIEMS is being extended over four decades to present time; GIEMS-D3 should then become available for this long time record too. For comparison with MGB model, monthly averages were considered for the period from 1999 to 2007.

SWAF-HR (Parrens et al., 2019) is a high-resolution (1 km) inundation data set derived from downscaling of the SWAF product specifically developed for the Amazon basin. The SWAF product (Parrens et al., 2017) is derived from the Soil Moisture Ocean Salinity (SMOS; Kerr et al., 2001) L-band passive microwave brightness temperatures (Al Bitar et al., 2017) with 3-day temporal resolution during the 2010-present period and has the significant advantage to detect water under dense vegetation. The SWAF-HR product was downscaled from its original resolution at 25 km to 1 km by using the Global Surface Water Occurrence from Landsat (Pekel et al., 2016) and the DEM Multi-Error-Removed-Terrain (MERIT DEM; Yamazaki et al., 2017). For comparison with MGB model, monthly averages were considered for the period from 2010 to August 2015.

Hess et al. (2015) surface water extent product (called hereafter Hess) is based on classification of Japanese Earth Resources Satellite-1 (JERS-1) Synthetic Aperture Radar (SAR) imagery for the years 1995–1996 (high and low water maps available) and is available at 90 m spatial resolution.

Time series of water level were acquired from 107 satellite altimetry virtual stations and 11 in situ gauges from ANA (Brazilian National Water Agency; available at <www.snirh.gov.br/hidroweb/>). Rivers satellite altimetry water levels time series were obtained from the THEIA/Hydroweb website. Data processing description can be found in Santos da Silva et al. (2010). Time series range from 2002 to 2010 and from 2008 to 2016 for ENVISAT and Jason-2 missions, respectively, and the estimated accuracy is around 10–40 cm. To complete the geographical validation, we manually processed three water elevation time series from the recently released Sentinel3-A mission at VSs (Virtual Stations) located in the wetlands (see Figure 9c for location of VS1, VS2, and VS3). The manual processing of the land products (SR_2_LAND) from Sentinel3-A SRAL mission was based on a simple filtering of high-resolution observations with a low backscatter coefficient, assuming that the SAR mode allows a low echo contamination. More information on S3-A altimetry mission can be found on the dedicated ESA website (available at <https://sentinel.esa.int/web/sentinel/user-guides/sentinel-3-altimetry>). A visual inspection was also performed to ensure that the selected high-resolution measurements come from the considered area. Although there is no overlap between the MGB run (1999–2015) and the S3-A data (mid-2016 to today), it is hoped that satellite altimetry provides an interesting insight on water levels fluctuations in the ungauged interfluvial areas. Finally, we used longitudinal profiles of surface water slope derived for 25 km long reaches for the Negro mainstem, the same used by Montazem et al. (2019). These data sets were obtained in two field campaigns with survey ships (25 September 2009 during falling limb and 17 October 2010 during low flow) and are available for the reach between São Gabriel da Cachoeira location to the confluence with Amazon River. A datum correction was performed to convert the observations into EGM96 datum through field measurements.

3. Results

3.1. 1-D Versus 2-D River Discharge

The MGB model rainfall-runoff parameters were calibrated based on discharge data from Caracaraí and Serrinha gauges, which are the most downstream stations along the Branco and Negro Rivers (except for Moura station, which is downstream of the Negro-Branco confluence), respectively. The calibrated rainfall-runoff parameters are provided as Supporting Information S1. Figure 3 presents simulated and observed discharges for the two gauges and shows an overall satisfactory agreement between both 1-D and 2-D observations. Nash-Sutcliffe efficiency coefficient (NSE) values were 0.76 (1-D) and 0.66 (2-D) at Caracaraí and 0.53 (1-D) and 0.53 (2-D) at Serrinha. The deviation between 1-D and 2-D models (RMSEr = 22%) is comparable to the errors between the models and observations (26%) in the Negro but are smaller in the Branco (29% against 41–49%). There is an overall discharge underestimation in the Upper Negro River which may be related to a biased TMPA precipitation in the region (Getirana et al., 2011). Simulated discharges suggest a higher hydrograph attenuation from river floodplains by the 1-D model in both Negro and Branco Rivers.

3.2. 1-D Versus 2-D River Water Levels

A spatial analysis of the performance of water level anomalies for all stations is shown in Figure 4a. Both 1-D and 2-D models have similar performance basinwide. The differences between 1-D and 2-D water level estimates are presented through a reach by reach analysis in Figure 4b. Deviation is relatively small, with most simulated reaches with RMSD <1 m for anomalies. On the other hand, absolute water levels indicate some discrepancies between the model estimates, with RMSD between 2 and 5 m for most reaches along the Negro River. RMSD values were smaller along upstream reaches and throughout the Branco River, which also presents smaller water level amplitude in comparison to the Negro.

Absolute water level time series along rivers (Figure 5) depict the overall coherence between 1-D and 2-D models in the Branco, where the deviation between them (RMSDr) is smaller than between model and observations. The opposite occurs with the Negro stations, with better agreement among models and observations than among them. The 1-D model has generally higher water levels in the Negro, which is associated to more floodplain storage as discussed in the next section. Water levels become more attenuated in the downstream parts of the Negro mainstem, which is also depicted by both models. On the other hand,

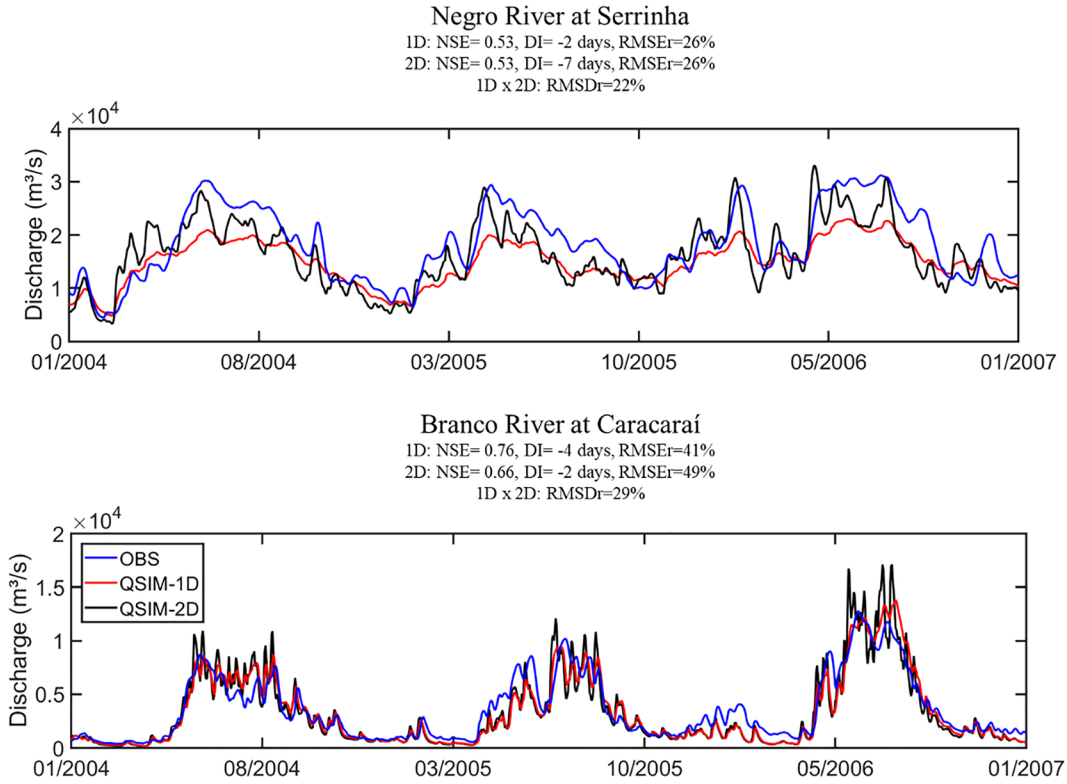

Figure 3. Observed and simulated discharges for the 1-D and 2-D MGB model versions for the in situ gauges Caracaraí and Serrinha.

RMSE values below 2 m as obtained here may be considered satisfactory given all uncertainties related to regional hydrodynamic models in poorly gauged basins as the Negro (e.g., DEM errors, simplified parameter calibration, and uncertain model forcing).

The water surface slope is also a very relevant hydrodynamic variable to define flood extent and fluxes. Figure 6 shows a comparison between simulated and observed water level slopes obtained in two field campaigns carried out during receding waters, for which RMSE values around 3.3–3.6 cm/km were obtained for both 1-D and 2-D. These errors are very high if compared with the average slope across the whole assessed profile (3.1 cm/km). Discrepancies between model and observations are higher than between 1-D and 2-D models (RMSD 1.9–2 cm/km), and errors are higher along the Negro-Branco confluence (chainage between 250 and 400 km) and in the Upper Negro River close to São Gabriel da Cachoeira (chainage larger than 700 km). The observed slope decreases around Barcelos (450 km; Figure 2), maintaining a plateau until Moura, which is located just downstream of the Negro-Branco confluence (chainage 250 km). Downstream of it, slopes sharply decrease to almost 0 cm/km close to the Amazon-Negro confluence at Manaus. While the latter reach is subjected to backwater effects from the Amazon (Meade et al., 1991), the reach between Barcelos and Moura is associated to the Mariuá fluvial archipelago, which has dozens of stable vegetated islands and is considered the largest in world (Montero & Latrubesse, 2013). Along the Branco-Negro confluence, just downstream of Mariuá, the Negro River width is largely reduced to around 2 km due to a delta feature, which was formed during Late to Mid Holocene period when the Branco River carried abundant suspended load, being a nonactive landform today (Latrubesse & Franzinelli, 2005). This region acts thus as a hydraulic control for upstream Negro reaches (i.e., creating backwater effects, as discussed by O'Loughlin et al., 2013).

Some hypotheses could explain the poor 1-D and 2-D estimates around upstream Negro and Branco-Negro confluence regions. Around the confluence, both models show a sharp decrease in water slope further upstream than it really is (near chainage 400 km). The adopted simple channel parameterization (i.e., regional geomorphic relationships between effective width and depth parameters and drainage area) provides

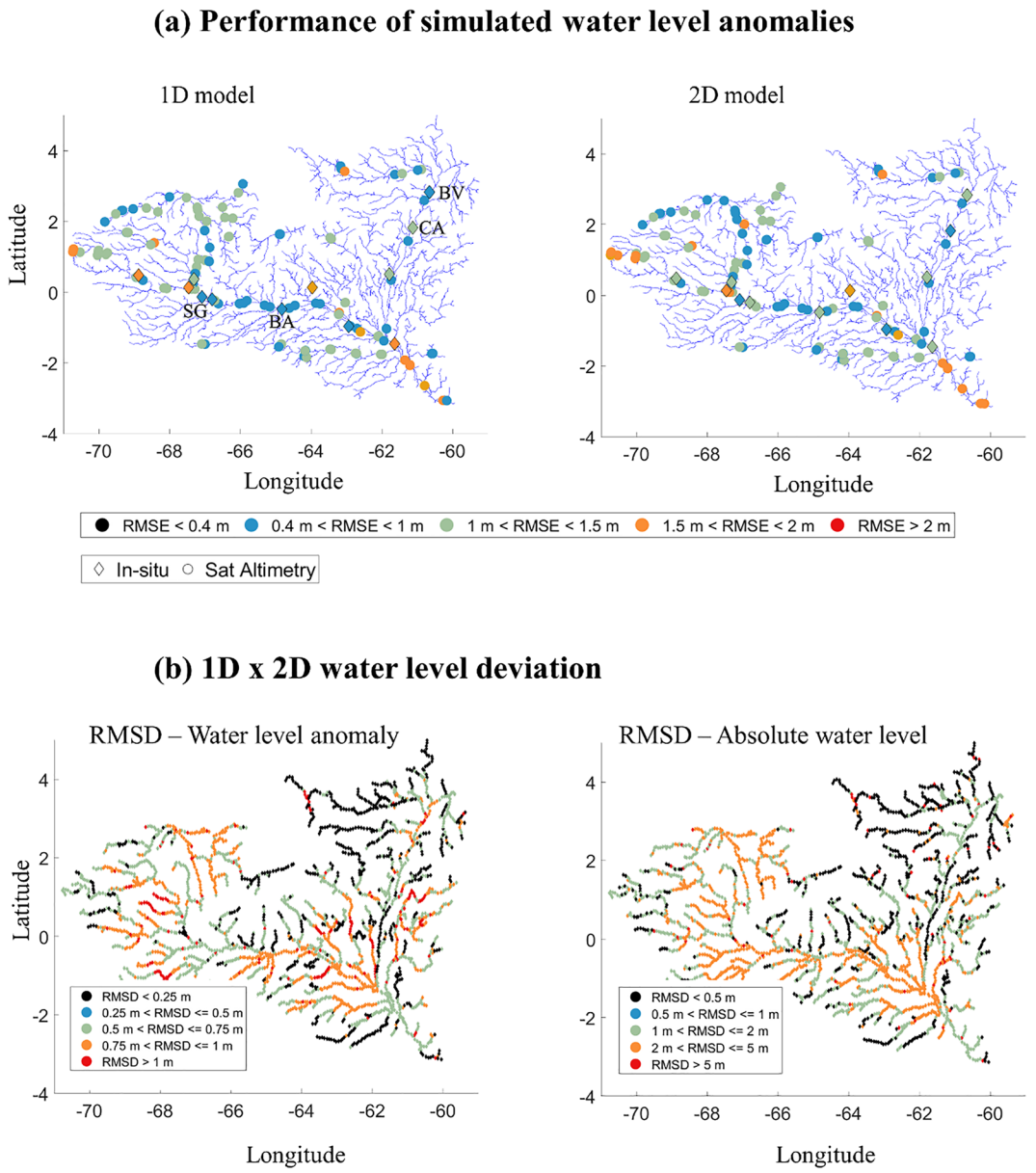

Figure 4. (a) Performance (RMSE) of 1-D and 2-D models for water level anomalies. Locations (see map in Figure 2) refer to SG: São Gabriel da Cachoeira; BA: Barcelos; CA: Caracaraí; and BV: Boa Vista. (b) Water level deviation (RMSD) between 1-D and 2-D models for anomalies and absolute water levels. Values presented only for drainage area >1,000 km^2 for figure readability. Please note that the scales have different ranges.

some explanation: Important changes on the river width (e.g., around the confluence region) were not represented in the model, so important hydraulic controls were not represented, which largely affects the simulated slopes (O'Loughlin et al., 2013) and should be addressed in future developments. The adopted coarse grid resolution (4–10 km) also hampers a proper representation of such local-scale (yet regionally relevant) features. Along the upstream Negro reaches, there is a somehow constant observed slope value throughout most of the river at around 4 cm/km, while simulation values reach values as high as 15 cm/km in certain reaches. This region is associated to rapids (Latrubesse & Franzinelli, 2005), and the relatively smaller river widths increase the DEM derived noises in the bed elevation parameter, possibly increasing the variation in simulated slopes. The adopted, simplified subgrid model conceptualization, which defines floodplain flows among cells, also adds some uncertainty to the slope representation.

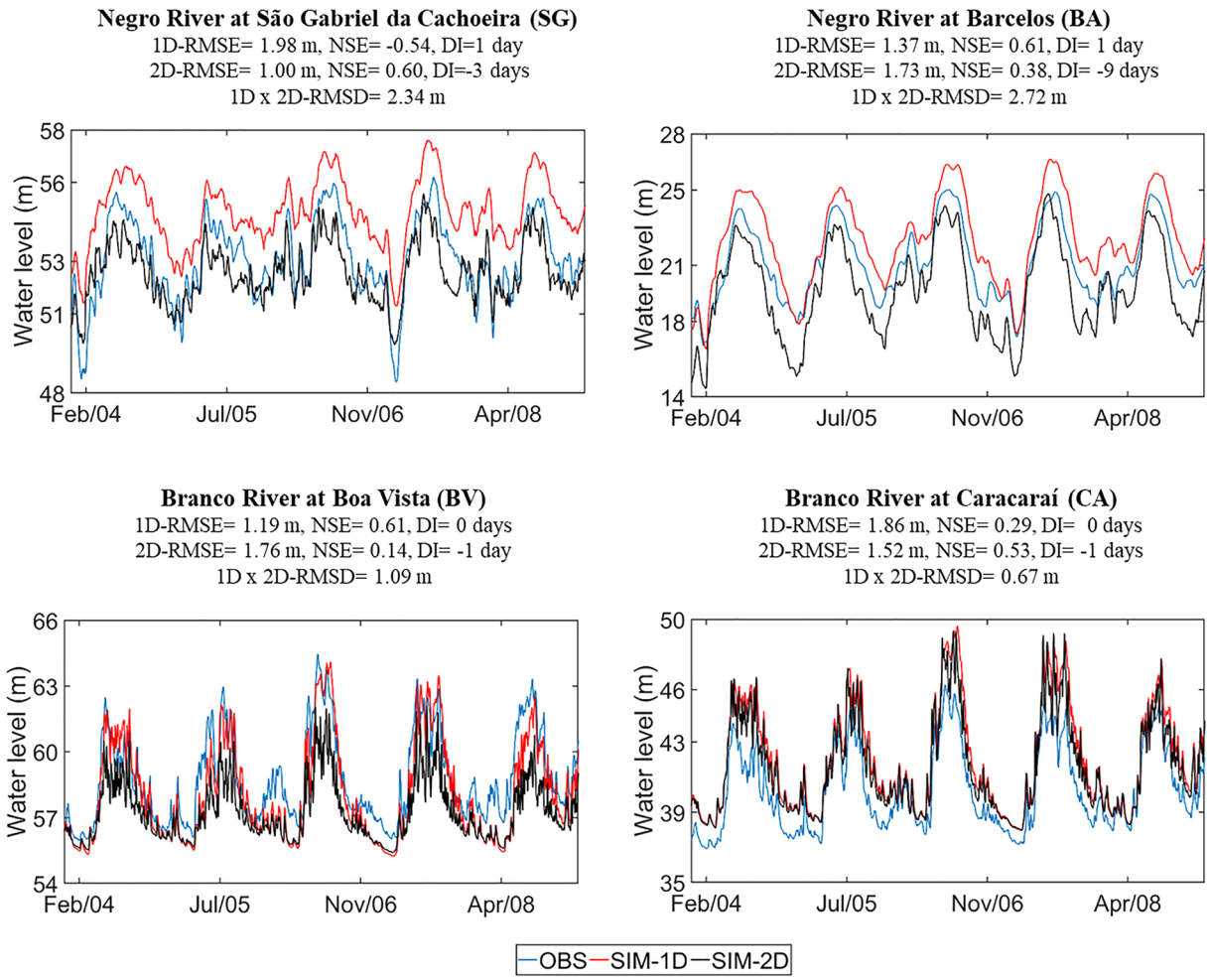

Figure 5. Absolute water level time series in Negro River at four locations across the basin (see location in Figure 4a).

Finally, there are also expected errors in the observed profiles, which were obtained during 10 days boat surveys (given the 900 km survey length) and are also subject to uncertainties related to Geoid model correction and GPS processing.

3.3. 1-D Versus 2-D Flood Dynamics Across Wetland Types

In this section, the differences between 1-D and 2-D models in representing the complex wetland dynamics in Negro River Basin are assessed. First, maximum flood extent estimates by the models and SWAF-HR, GIEMS-D3, and Hess remote sensing products are compared in Figure 7. There is an overall good spatial agreement between all estimates, particularly considering the uncertainties existent in the adopted methods and the different mapping period for each data set (2000–2015 for MGB, 1995–1996 for Hess, 1993–2007 for GIEMS-D3, and 2010–2016 for SWAF-HR). The CSI metric (Equation 9) for flood extent spatial assessment (Table 1) indicates that all data sets have similar spatial coherence with the modeling outputs, for both interfluvial and mainstem wetlands, while the spatial agreement between 1-D and 2-D (37% and 76% for interfluvial and mainstem, respectively) was higher than between models and remote sensing data sets. On the other hand, the 2-D model shows a poorer performance in comparison to 1-D, which in turn was associated to more flooding than the 2-D (overall bias between 11% and 18%). It must be noted that the 2-D model is dependent on the definition of which 2-D wetland cells have river channels—in this study, the intersection between Hess product with the drainage network by Seyler et al. (2009) was used (Figure S1d). Smaller river floodplains are represented in MGB and Hess but to a lesser extent in SWAF-HR and GIEMS-D3. This is mainly due to the fact that Hess product comes from truly native high-resolution "direct" observations

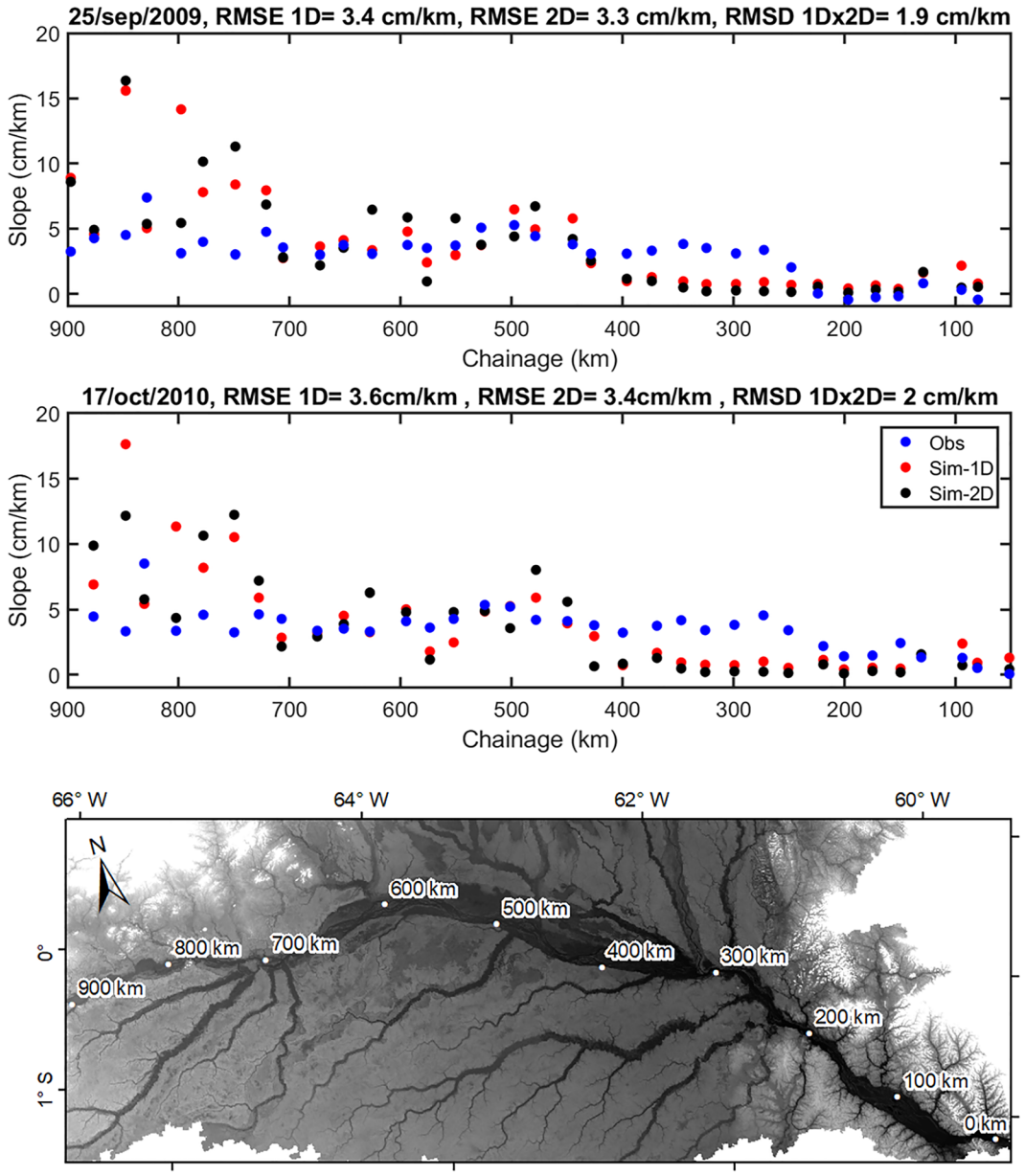

Figure 6. Simulated and observed longitudinal water level slope profiles for the Negro mainstem for 25 September 2009 and 17 October 2010. Chainage is the distance from the basin outlet (at Manaus), as presented in the bottom figure map.

while GIEMS-D3 for instance is downscaled from a low-resolution global product (GIEMS) which is known to have limitations in capturing small water bodies (see Figure 7 of Prigent et al., 2007 for a comparison between GIEMS and Hess over the Amazon). Wetlands in the southern side of the Negro mainstem (as the Cuini wetland; Belger et al., 2011; Figure 2b) are not mapped by SWAF-HR because of radio frequency interference (RFI) and topography effect filtering, while across the basin, GIEMS-D3 depicts less smaller size river floodplains than SWAF-HR.

Flood extent time series for the interfluvial wetlands and the Negro mainstem regions (Figure 8 and Table 1 for metrics) indicate a higher agreement between MGB and SWAF-HR for the interfluvial wetlands (RMSE 24% to 31%; correlation 0.82 to 0.87; bias −5% to 2%) than between MGB and GIEMS-D3. For the mainstem, there is a similar performance in terms of RMSE between MGB 2-D and SWAF-HR (21%) and GIEMS-D3 (17%), while MGB 1-D is in better agreement with SWAF-HR (14%). The time series show that MGB,

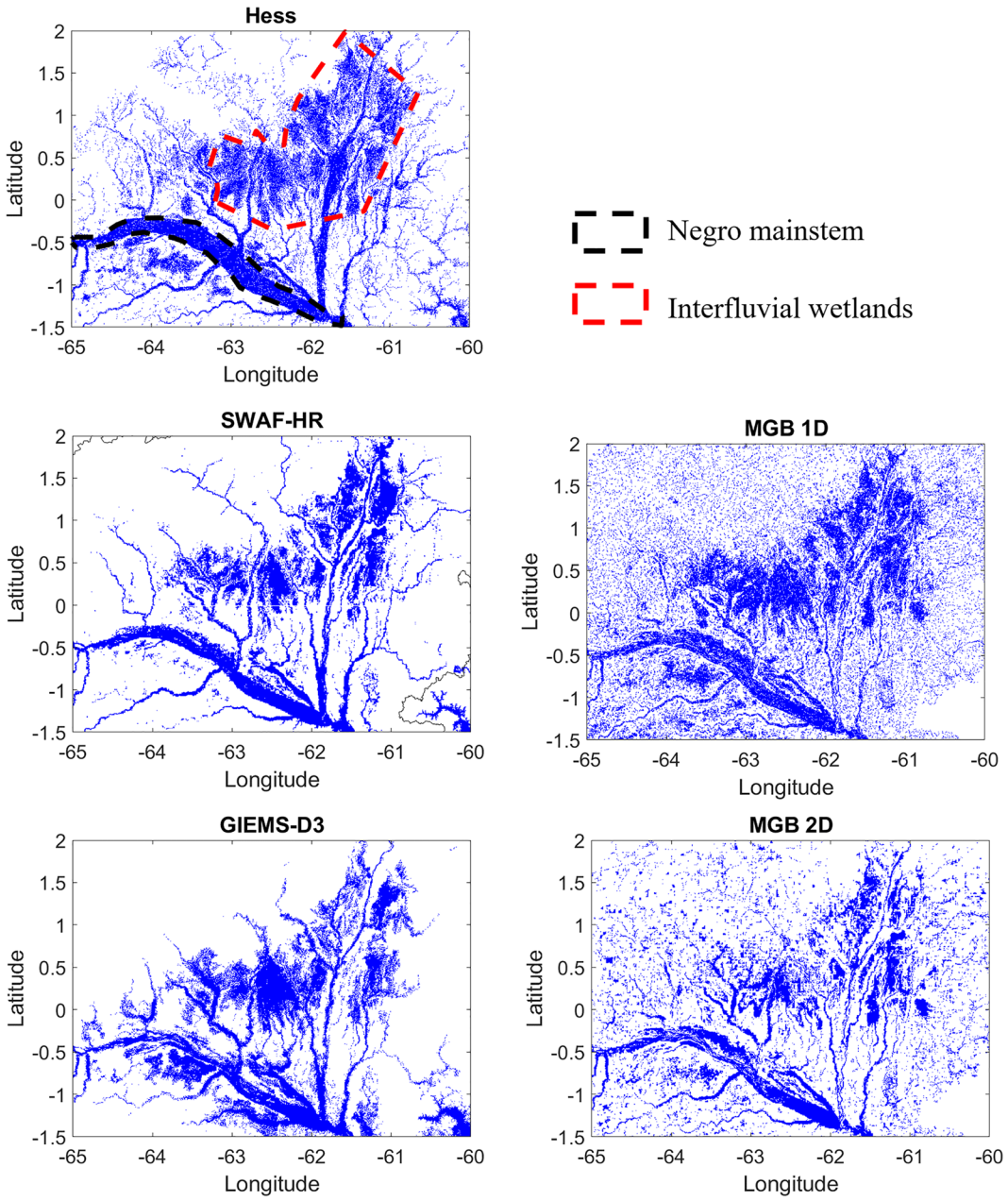

Figure 7. Maximum flood extent maps from 1-D and 2-D MGB model simulations and remote sensing based products (Hess, SWAF-HR, and GIEMS-D3) in the Central Negro River Basin.

GIEMS-D3, and SWAF-HR estimates are contained within the maximum–minimum range of Hess product (green lines), except for dry years in SWAF-HR and most dry periods in GIEMS-D3. Additionally, SWAF-HR indicates that the minimum annual flood extent decreased during the last 3 years due to an intense drought that affected the region (Parrens et al., 2019), while MGB represents this effect to a lesser extent. The smallest errors are found between MGB 1-D and SWAF-HR in both mainstem and interfluvial areas, and deviations between 1-D and 2-D models are generally similar to the errors in relation to remote sensing products. Regarding flood extent range, MGB 2-D has a smaller amplitude than 1-D in the interfluvial areas and a similar one in the mainstem. In turn, GIEMS-D3 indicates a relatively small amplitude along the Negro mainstem but a similar range in the interfluvial wetlands.

Table 1
Performance Metrics Between Simulated and Observed Flood Extent Time Series (RMSE/RMSD, r, and Bias) and Maximum Extent (CSI) for Three Remote Sensing-Based Products (GIEMS-D3, SWAF-HR, and Hess) and Two Model Types (MGB 1-D and 2-D)

	Interfluvial wetlands						
	1-D validation			2-D validation			
	GIEMS	SWAF	Hess	GIEMS	SWAF	Hess	1-D × 2-D
RMSE/D	59%	24%	—	46%	31%	—	27%
r	0.58	0.82	—	0.65	0.87	—	0.89
Bias	55%	2%	—	34%	−5%	—	11%
CSI	43%	44%	44%	25%	24%	23%	37%
	Negro Mainstem						
RMSE/D	27%	14%	—	17%	21%	—	25%
r	0.59	0.79	—	0.74	0.75	—	0.75
Bias	19%	3%	—	−3%	−14%	—	18%
CSI	66%	72%	74%	63%	64%	62%	76%

Simulated flood volume (Figure 8b) reveals additional interesting aspects on the wetlands dynamics. The overall behavior of 1-D and 2-D models is similar to the one obtained for flood extent, that is, the 1-D has more flood volume than the 2-D in the interfluvial wetlands, and it is similar in the mainstem. However, one must notice the magnitude and flood season length differences between both regions. While in the interfluvial areas flood extent varies between 4,600 (5,700) km^2 and 21,000 (15,000) km^2 for the 1-D (2-D) model, it ranges from 2,700 (2,900) km^2 to 7,810 (7,760) km^2 in the mainstem. For flood volume, the ranges are 8.6 (6.1) km^3 to 43 (29) km^3 for interfluvial and 12 (11) km^3 to 45 (46) km^3 for mainstem. This shows that flood volume magnitudes are similar between both areas, and since the interfluvial areas have a larger total flood extent, water depths are far higher in the Negro mainstem river. Additionally, satellite altimetry virtual stations indicate that water levels have an annual amplitude between 0.3 and 1.0 m in interfluvial wetlands but may reach up to 8 m in adjacent rivers (Figure 9a). It is worth noting that the absolute amplitude of the water surface elevation variation may be slightly underestimated due to the 27-day temporal sampling of the S3-A mission. The 2-D model is able to represent the small water level variation in interfluvial areas, while the 1-D implementation, which has river channels in all its computational grids, has amplitudes higher than 1 m in all virtual stations. Interestingly, this is in contrast with the Negro mainstem, for which the 2-D model had less attenuation and thus a higher amplitude.

Simulated transects for the maximum water level (Figure 9b) stress the higher connectivity ensured by the 2-D model, which has less variation in its water levels in comparison to the 1-D one (e.g., along the Negro mainstem between distances 0.5° and 1°). This occurred because of the existing connection among all neighbor 2-D cells, in comparison to the single upstream-downstream connectivity in the 1-D simulation.

Finally, 2-D model outputs were used to estimate floodplain flow directions across the different wetland types for a high water period (Figure 10). While the 1-D model simulates floodplains as storage units and computes channelized flow along the single upstream-downstream connectivity direction, the 2-D model allows floodplain flows among all orthogonal neighbors and channelized flow among all neighbor cells with a predefined channel. Figure 10 shows how the drainage of interfluvial wetlands (details in Figures 10b and 10c) occurs with a diffuse pattern, although there are channels that ultimately drain the wetlands, leading to a flow convergence toward them. The 2-D flow direction is largely dependent on the terrain elevation, so the wetland in Figure 10b is mainly drained through the Demini River (large downward yellow arrows) but also through other adjacent rivers. The 1-D model, however, did not represent correctly this pattern. Since the 1-D drainage network was automatically derived with a GIS technique, it can create a wrong stream definition in some regions (especially the flat ones). For the case of the Demini River, it was delineated as if it was a small river flowing northward, so the main river draining the interfluvial area was the (incorrect) south tributary located in the center of the figure (thick blue line). As a consequence, the smaller drainage capacity of the interfluvial wetlands led to the higher estimated flood volume with the 1-D model. This highlights the potential errors that may arise with GIS preprocessing steps, which could be corrected with a DEM processing technique (e.g., burning the DEM with the correct drainage), but which are also avoided when the 2-D model is employed. Finally, the highest floodplain flows in the Negro basin occur along the river mainstem, especially along the Mariuá archipelago near the Negro-Branco confluence.

3.4. 1-D Versus 2-D Model Sensitivity to Hydrodynamic Parameters

To further understand the differences between 1-D and 2-D models, a local, one-at-a-time sensitivity analysis of model estimates to hydrodynamic parameters is performed by altering the following parameters: channel bankfull depth, width and length, channel and floodplain Manning coefficients, and floodable areas (i.e., the area from the stage-area relationship used to estimate floodplain storage and conveyance) (Figure 11). The assessed variables are basin outflow, water level at Moura location, and flood extent in interfluvial wetlands. All values were altered from −50% to +50% of its default value, except for floodplain Manning friction, which

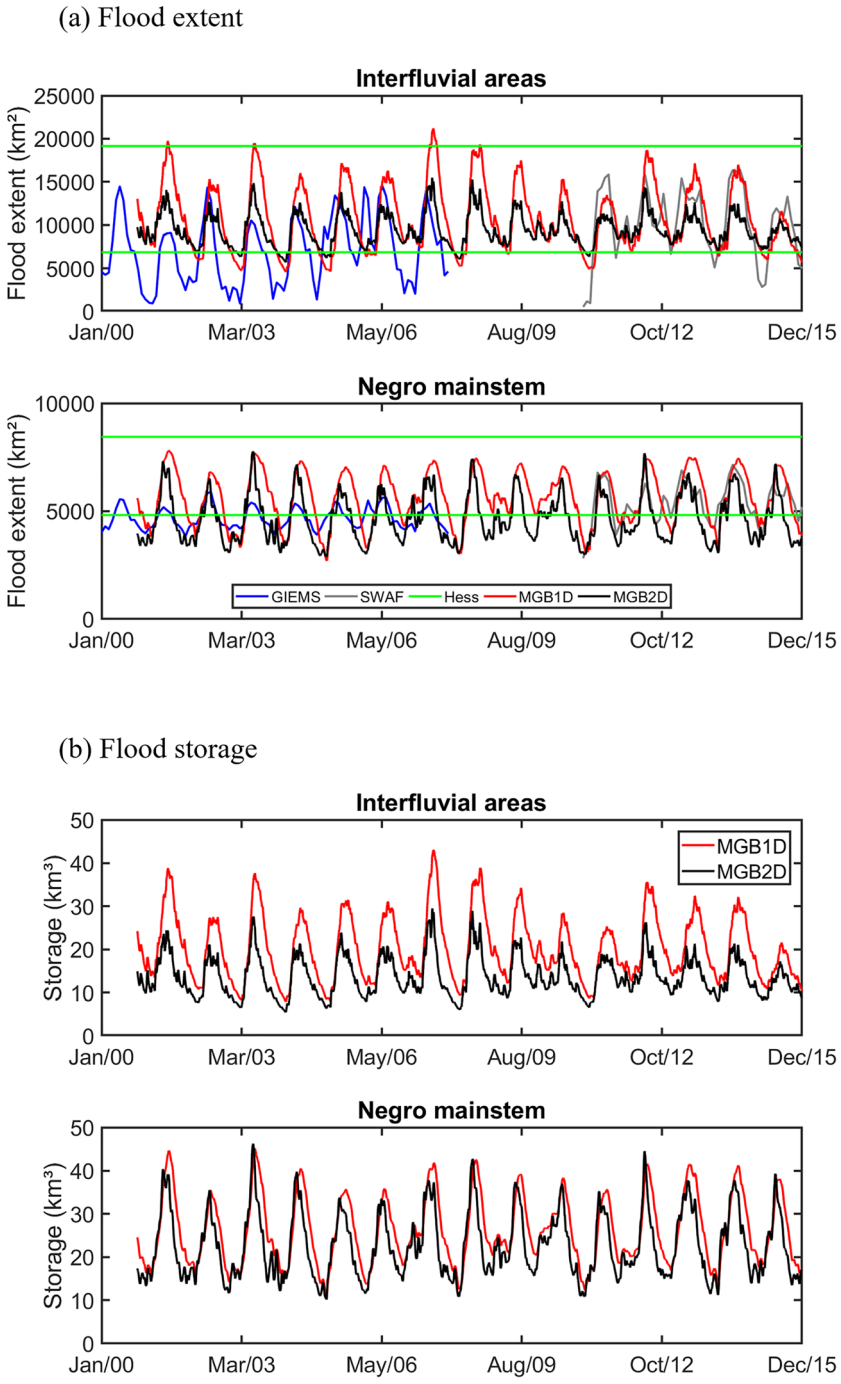

Figure 8. Time series of (a) flood extent and (b) volume in the Negro mainstem and interfluvial wetlands.

were varied from −50% to +500% (i.e., from 0.05 to 5). The large range of the latter parameter was chosen because of its uncertainties and the interest on analyzing the effect of floodplain storage, since a very high floodplain roughness value would make the 2-D model closer to the 1-D with storage floodplain unit.

For discharge and flood extent, the 2-D model presented a smaller sensitivity than the 1-D to all parameters (with the exception of floodplain Manning, which only varied in the 2-D model since the 1-D has storage floodplain units). In turn, water levels had similar estimated uncertainties for 1-D and 2-D.

For the ±50% range, channel width, depth, and Manning led to the highest uncertainties in all variables, followed by channel length and then floodable areas. The 2-D model had a small sensitivity to floodplain

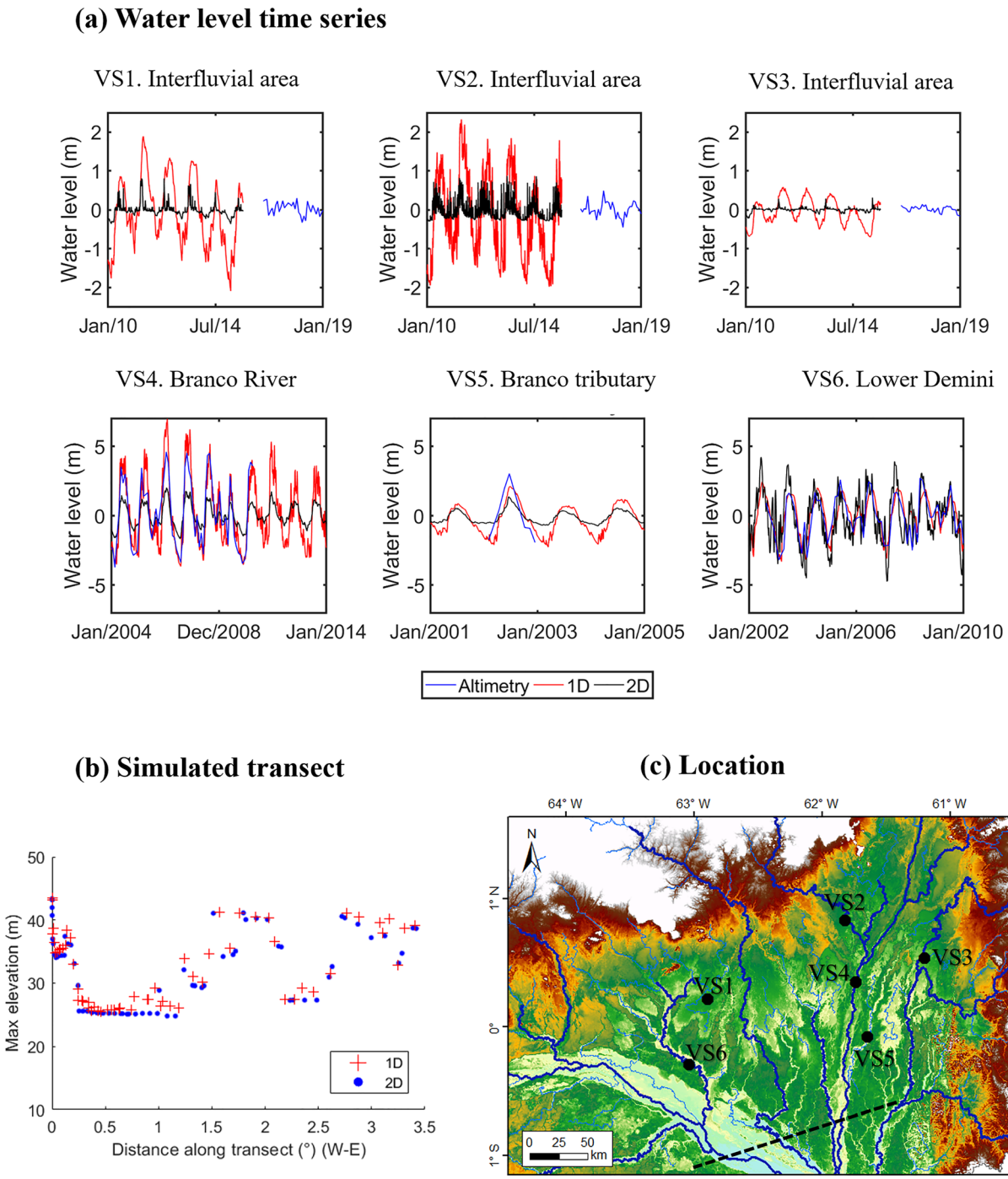

Figure 9. (a) Water level anomaly (i.e., water level subtracted by the long-term average) time series (simulation and altimetry) for six locations across the Negro basin: three virtual stations located in interfluvial areas (VS1, VS2, and VS3) and three along rivers (VS4, VS5, and VS6). Vertical and horizontal scales are different between the upper and lower figures. (b) Maximum simulated elevation along a transect (dashed black line in panel (c)) for 1-D and 2-D models. (c) Location of the virtual stations and transect. Only large rivers are presented in the drainage network for figure readability.

Manning. The reported sensitivity for the 1-D model width, depth, and Manning parameters is similar to the values presented by Paiva et al. (2013) and Yamazaki et al. (2011) for 1-D hydrodynamic regional models.

For flood extent, the smaller sensitivity of the 2-D model occurs due to its higher capacity to drain out flood waters, while altering 1-D parameters leads to biases in the estimated flood extent. Results are similar for Negro mainstem flood extent and are not presented here for brevity.

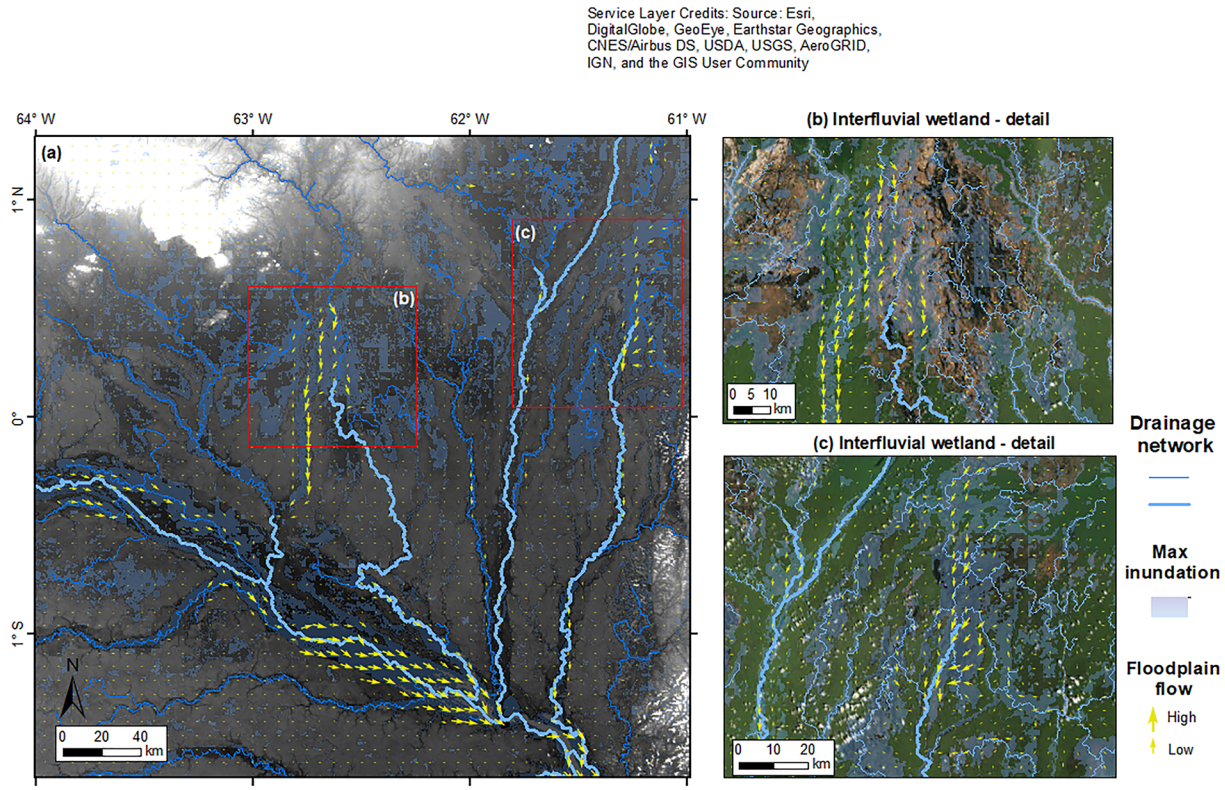

Figure 10. (a) Simulated 2-D floodplain flow direction and magnitude across interfluvial wetlands and Negro mainstem during high water period (19 June 2003). Source of satellite images on panels (b) and (c): Esri, Digital Globe, GeoEye, Earthstar Geographics, CNES/Airbus DS, USDA, USGS, AeroGRID, IGN, and the GIS User Community (Esri, 2009).

Within the assessed range, with different parameter values both 1-D and 2-D can yield similar estimates. For instance, a channel Manning value reduction of 50% would lead to an increase in discharge (i.e., the upper bound values of 1-D estimates in Figure 11) that would make the 1-D estimate very close to the 2-D one. This shows the higher drainage capacity of the 2-D model since a decrease in 1-D Manning is necessary to achieve a similar performance. It is important to stress, on the other hand, the equifinality problem existent in Manning parameterization, which must be taken into account to attain realistic model estimates.

3.5. On the Coupling Between Hydrological and Hydrodynamic Processes

The developed 1-D and 2-D MGB modeling approaches allow a coupling strategy between hydrological and hydrodynamic processes, through (i) infiltration from flooded areas into adjacent unsaturated soils (the default parameter KINF = 20 mm/day was adopted for simplicity, see Fleischmann et al., 2018) and (ii) evapotranspiration computation considering the variable cell flooded fraction. In this section, simulation tests with and without these two mechanisms are analyzed.

Evapotranspiration over the whole basin (Figure 12) shows that the 1-D model has higher rates than the 2-D when open-water evaporation of flooded areas is considered. The scenario without dynamic evapotranspiration (i.e. NoETw, solid lines), that is, considering evapotranspiration as if the cell had no flooding areas, indicates that the 1-D rates would be smaller and similar to the 2-D NoETw estimates. These lower ET rates would lead to higher discharges in the Negro River at Serrinha (red solid lines in Figure 12), which is already subjected to floodplain effects at this location, and smaller differences in the Branco River at Caracaraí, less subjected to flood storage. Differences among evapotranspiration estimates are smaller in 2-D than 1-D due to smaller flooded areas, which is also reflected on the simulated discharges. In turn, the effect of infiltration from flooded areas is practically negligible. Different infiltration parameters were tested (a large range between 0 and 40 mm/day as in Fleischmann et al., 2018) and led to a similar conclusion.

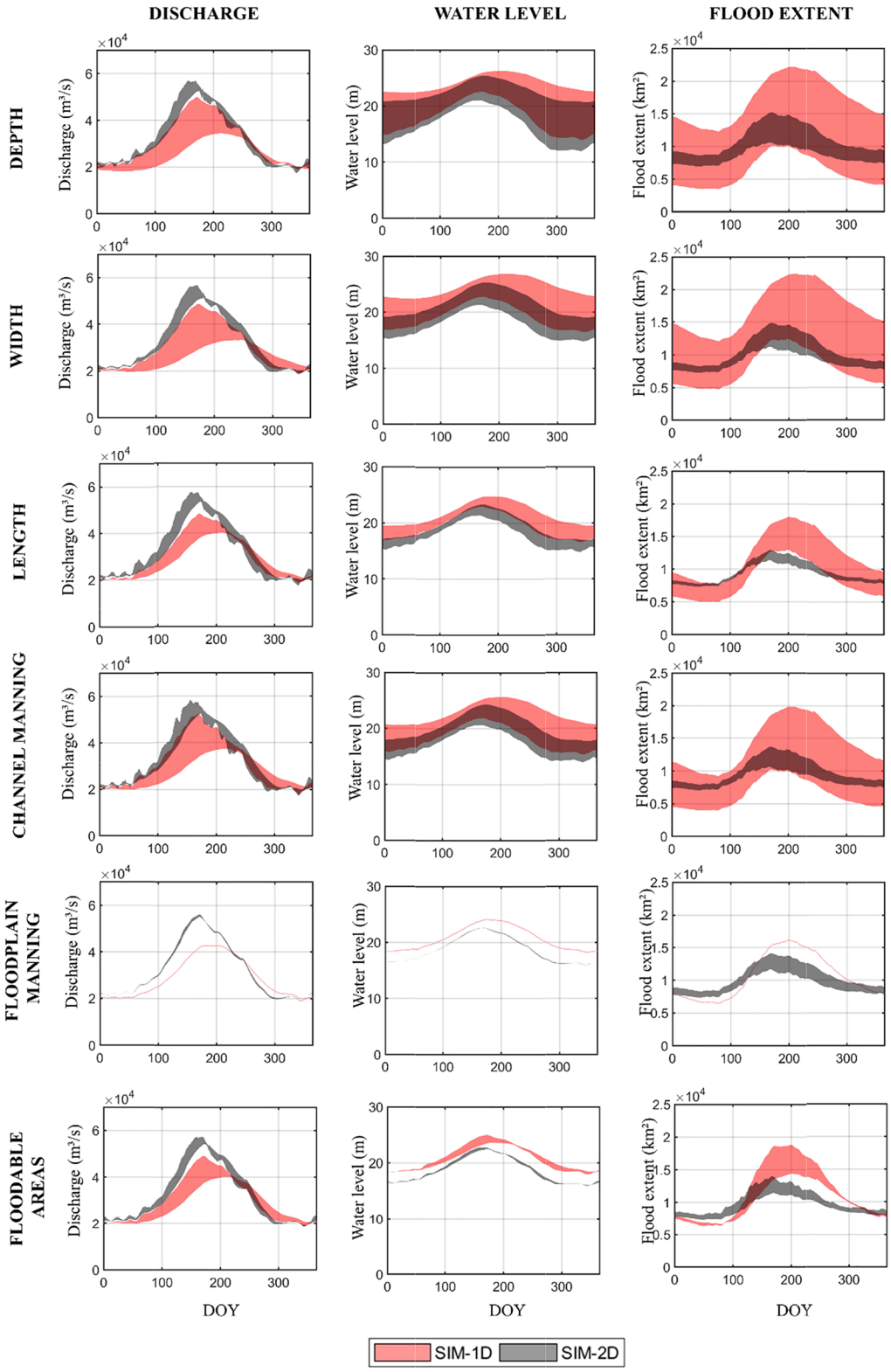

Figure 11. Variability of 1-D and 2-D simulated variables (discharge, water level at Moura location, and flood extent of interfluvial wetlands) to alterations in hydrodynamic parameters (values changed from −50% to +50%): channel bankfull depth and width, channel length, channel and floodplain Manning coefficients, and floodable areas (i.e., the area from the stage-area relationship used to estimate floodplain topography storage). Floodplain Manning is evaluated for the range between −50% and +500% and only for the 2-D model, since the 1-D adopts storage floodplain units.

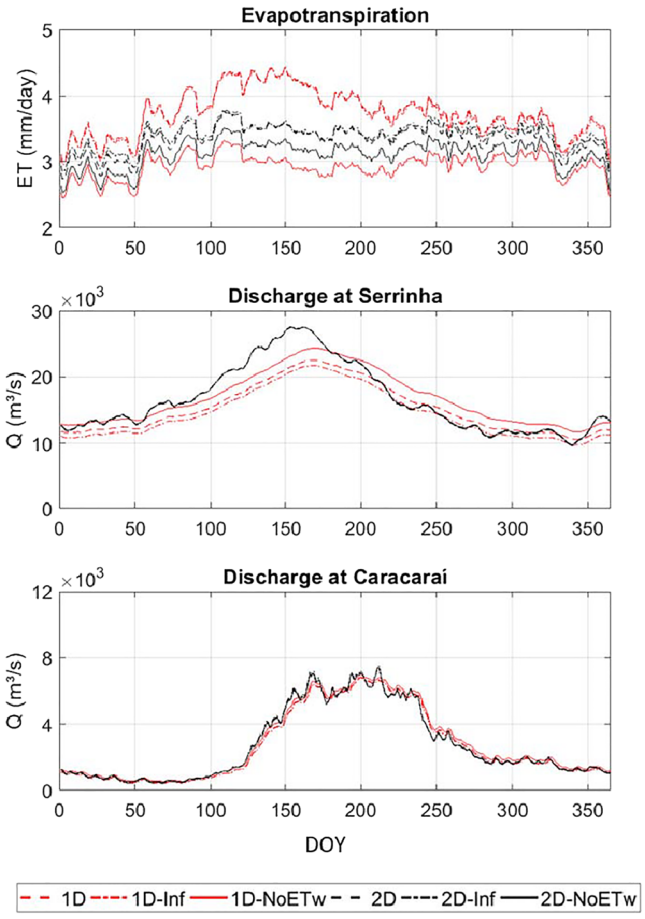

Figure 12. Analysis of the coupling between hydrologic and hydrodynamic processes for simulated evapotranspiration and discharge (Negro River at Serrinha and Branco River at Caracaraí) for the scenarios default (with open water evaporation and without infiltration), "Inf" (with infiltration from floodplain into soil), and "NoETw" (without flooded areas open water evaporation).

4. Discussion

4.1. 1-D Versus 2-D Hydrodynamic Model Estimates: Comparison and Uncertainties

In this study, a comprehensive comparison between 1-D and 2-D approaches applied at regional scale (~700,000 km^2) was performed. A simplified, local sensitivity analysis with one-at-a-time parameter variation (Pianosi et al., 2016) was performed due to computational constraints, as done by previous studies of regional/continental models (Decharme et al., 2008; Paiva et al., 2013; Yamazaki et al., 2011). This study focused on hydrodynamic modeling only, so the uncertainty in the rainfall-runoff generation process was not assessed. However, it must be recognized that part of the mismatch between simulation and observation come from uncertainty in the runoff estimates, for which the input precipitation is usually assumed to lead to the highest uncertainties (Liu et al., 2012). This is certainly the case for the Negro basin where rainfall rates are among the highest in the Amazon and associated to major uncertainties (Getirana et al., 2011). Recent studies have discussed the role of runoff (and other water balance components) uncertainty on regional hydrodynamic models (Bermúdez et al., 2017; David et al., 2019; Grimaldi et al., 2019). Adding to this literature, we have performed tests on the role of an online (two-way) coupling between hydrologic and hydrodynamic processes. Considering a dynamic evapotranspiration and infiltration from floodplains into soils did not lead to major impacts on both 1-D and 2-D estimates, and model dimensionality and parameterization were more important in defining differences between the models. This is in accordance with Paiva et al. (2013) for an application in the Amazon, where soils are often wet, making vegetation ET close to open water evaporation and reducing the coupling relevance. A higher impact of the coupling approach is expected for wetlands as the Pantanal (Da Paz et al., 2014), Okavango Delta (Bauer et al., 2006), and Niger Inner Delta (Fleischmann et al., 2018). The latter, for instance, is a semiarid wetland where the interaction between wetlands and regional climate is very relevant (Taylor, 2010). The online coupling also requires a proper parameterization of open water evaporation (Penman equation in our case) as well as wetland infiltration capacity, which is complicated in large ungauged wetlands. This, however, suggests that more research should be performed to better understand how feedbacks occur between wetlands and the adjacent soils and atmosphere, for example, by using micrometeorological and eddy-covariance flux towers across wetland systems (Borma et al., 2009).

Both 1-D and 2-D MGB models were capable of estimating satisfactory discharges and water levels along major rivers. Major differences occurred between 1-D and 2-D models for flood extent and volume estimates. The 2-D model generally led to less flooding (lower flood extent and flood volume and less attenuated discharges), due mainly to an enhanced drainage capacity through floodplain and channel cells. Changes in parameter values mainly altered the flood extent during high water periods, while low water values remained similar. In turn, the 1-D led to far more flooding than the 2-D (i.e., it totally filled the interfluvial depressions), and it was also more sensitive to hydrodynamic parameters.

Regional-scale models differ from the reach scale ones through coarser resolution and typical subgrid approach. The decoupled formulation presented here has been called 1.5-D or quasi-2-D and usually do not represent momentum transfers at confluences, while proper 2-D models should be able to account for local-scale processes as recirculation zones and mixing layers and more localized head losses (Chen et al., 2018), associated, for example, to local-scale floodplain obstacles and channel bends. In this study, a 4 km spatial resolution was adopted, which is in accordance with current regional models for continuous simulation (O'Loughlin et al., 2020). Increasing resolution will not necessarily improve model performance

(Bernhofen et al., 2018; Dottori et al., 2013), and at different scales, different processes will be represented, and diverse parameter values are likely to be required. Mateo et al. (2017) evaluated the bifurcation scheme of 1-D CaMa-Flood (Yamazaki, Sato, et al., 2014), which was developed to better represent complex wetlands with 2-D flow patterns. They concluded that this implementation led to flow connectivity and maintained flow capacity within river floodplains at different model resolutions. The CaMA-Flood 1-D model with single upstream-downstream connectivity had restrictive flow directions, and when a fine resolution was applied, excessive backflow occurred in lateral tributaries, while the bifurcation scheme did not lead to it. These results are in accordance with the ones obtained in this study. Besides, this study showed that the 2-D model was less sensitive to hydraulic parameters than the 1-D. This suggests that, even with relatively similar outputs, the former could be preferred to be adopted, especially considering the uncertainties inherent to large-scale model parameterization. Smaller variability in 2-D predictions in relation to 1-D was also found elsewhere (Cook & Merwade, 2009).

More attention should be paid for uncertainties on regional model structure. For example, a few studies have addressed the definition of subgrid flow parameters. Although subgrid methods are used in all scales (Casulli & Stelling, 2011), for example, porosity parameters in urban flood models to simulate building effects on storage and conveyance (Dottori & Todini, 2013; Sanders et al., 2008), particular settings are adopted for regional models. In this study, 2-D channel flow was allowed between all neighbors (D8), while others have adopted a D4 direction (Neal et al., 2012). Upscale of flow directions algorithms (Paz et al., 2006) could be adopted to estimate channel flow with a single upstream-downstream connectivity, especially where wetland diffuse flow does not occur. 2-D floodplain flow width was defined based on the connected pixels at each cell face, while other models adopt different strategies for it, for example, flooded area divided by cell length (Getirana, Peters-Lidard, et al., 2017). The effect of not properly considering channel length within a cell must also be addressed (Paz & Collischonn, 2007). In this study, the vector-based 1-D model yielded less uncertain river lengths for major rivers in comparison to the 2-D one with flow slope based on the cell size.

4.2. On the Capability of 1-D and 2-D Models to Simulate Different Wetland Types

For comparisons between hydrodynamic models, it is fundamental to consider wetlands with contrasting hydraulics (Bernhofen et al., 2018). The Negro River Basin is an interesting case study for understanding the capability of regional hydrodynamic models to represent processes at varying wetland types. While river floodplains typically have high water level variation and volume derived from both local and upstream catchments, interfluvial wetlands are more dependent on local runoff and rainfall (Junk et al., 2011; Reis et al., 2019) and present smaller water level amplitudes. The way that 1-D and 2-D models represent these divergent flows defines the overall capacity of each one to simulate flood dynamics. Furthermore, the diverse wetlands may have different sensitivity to extreme events. For instance, a recent drought has caused a large decrease in the Negro interfluvial wetlands flood extent (see the decrease in SWAF-HR estimates during the last 3 years in Figure 8a), while the floods along the mainstem, which respond to a much larger upstream drainage area, seemed to be less impacted. The hydrological regime in interfluvial wetlands may also be less impacted by human alterations in the mainstem than in river floodplains, given the smaller surface connectivity between mainstem and interfluvial areas. However, this hypothesis must be further assessed, including possible wetland-groundwater interactions and especially considering the current scenario in the Branco River Basin, where a large dam is planned to be built in the next years (Latrubesse et al., 2017).

Our results show that 1-D and 2-D models respond differently for each wetland type, while 1-D and 2-D models had similar performance for flood extent and volume, discharges, and water levels in the Negro mainstem, the main difference related to the interfluvial wetlands. 1-D models are developed for river floodplains, and they are expected to be sufficient for large-scale in-channel river hydrodynamics only (Schumann et al., 2013). They have typically adopted floodplains as storage units, although exceptions do exist (Getirana, Peters-Lidard, et al., 2017).

Along the interfluvial wetlands, no channel dominates the flow pattern, so the consideration of channels in the 1-D model led to high and erroneous water level amplitude (Figure 9). The 2-D model was able to reproduce the small amplitude (<1 m) which is characteristic of rain-fed wetlands. An interesting future validation for such poorly gauged wetlands relates to fusing model estimates with remote sensing, swath-based water level estimates (Alsdorf et al., 2007; Cao et al., 2018; Kim et al., 2017) and assessing the assumption of a horizontal water level in the models' cells. In our modeling framework, following the current

state-of-the-art regional scale models, water level was assumed horizontal within a model unit (~4 to 10 km). Although a high-resolution 2-D model (e.g., 90 m) may correctly represent the heterogeneous water surface elevation reported in floodplains (Alsdorf, 2003), this is certainly not the case of coarse resolution 1-D and 2-D models.

The 1-D model could not represent the drainage that occurs along the interfluvial wetlands, so water storage was erroneously large. With the 1-D model, the wetland behaved as a laterally constrained floodplain (in the sense of Hunter et al. (2007)). The 2-D regional model also enhanced connectivity (especially for large wetlands), as showed for the Negro mainstem, which is in accordance with recent regional hydrodynamic model studies (Altenau et al., 2017; Bernhofen et al., 2018; Fleischmann et al., 2018; Mateo et al., 2017; Neal et al., 2012). This study outcomes are relevant for the modeling of other basins such as the Congo (Revel et al., 2019; Tshimanga & Hughes, 2014), which presents complex hydraulic controls (O'Loughlin et al., 2013) and interfluvial wetlands (Jung et al., 2010; Kim et al., 2017; Yuan et al., 2017) along the large Cuvette Centrale that are still poorly understood.

Water storage is a fundamental variable to understand global biogeochemical cycles and wetland water balance and to foster water resources and flood risk management related to climate variability (Frappart et al., 2014, 2012, 2005; Papa et al., 2013; Schumann et al., 2016; Yuan et al., 2017). In the case of the Negro basin, flood storage is generally smaller in interfluvial wetlands due to smaller water depths than river floodplains. Both 1-D and 2-D models agreed on it, although 1-D seemed to overestimate floods in the former. The structure of 1-D models is designed for river floodplains, and complex wetlands with diffuse patterns and many outflow drainage channels may lead to overestimation of flood storage. On the other hand, the 2-D model applied here suggested that flood storage was too small, and a better parameterization could perhaps be achieved, for example, by refining the definition of cells without channel flows (Figure S1d).

Finally, discrepancies between flood extent estimated by models and remote sensing highlight the importance of better understanding and considering the uncertainties inherent to each classification method. Part of the disagreement is related to the fact that the remote sensing products are not fully consistent among themselves. Also, data sets driven by passive microwave observations (GIEMS-D3 and SWAF-HR, typically of ~25 km spatial resolution before being downscaled) have difficulties to retrieve very small wetlands due to the inherent low resolution of original data (Parrens et al., 2019; Prigent et al., 2007), while the models and SAR based products can better achieve this. Small allocation errors or noise can slightly change the results, even if the overall pattern is satisfactory. The better agreement between model and SWAF-HR may be explained by the fact that the latter uses an improved DEM (MERIT) in comparison to GIEMS-D3. Since MGB also uses MERIT as auxiliary information, it might reinforce the agreement with SWAF-HR. Furthermore, SWAF-HR was developed specifically for the Amazon (as is Hess product), so it is expected to have a better performance than global products as GIEMS-D3. Comparison and validation of flood extent is not trivial because of the lack of in situ data. The conclusions here should be considered with care as the remote sensing data sets do not all cover the same time period and one of them was used for model calibration (i.e., Hess map to define 2-D cells without channels).

4.3. Toward Better Estimates With 1-D and 2-D Regional Hydrologic-Hydrodynamic Models

The choice between 1-D or 2-D physically based models to realistically simulate river-wetland processes depends on the scale and variables of interest and the intended application with its required accuracy (e.g., environmental impact assessment, flood hazard studies, and biogeochemical and sediment estimates). Data availability is also a fundamental element of decision, since good DEMs are required for accurate, locally relevant 2-D flood modeling, but seem to be less important for 1-D models that aggregate floodplain storage within coarse units (Fleischmann et al., 2019). Our results showed that the type of wetlands being simulated is also relevant: A river floodplain can be satisfactorily represented by both 1-D and 2-D approaches for variables as discharges, water levels, and flood extent, but interfluvial wetlands, which are less connected to the main river systems, would require a 2-D approach, given the nature of the diffuse flow pattern. Besides, given that the 2-D scheme was less sensitive to most hydraulic parameters than the 1-D one, it could be chosen preferably. The higher 2-D computational cost is also relevant, since it computes flows across all neighbor cells and not only along upstream-downstream direction as in the 1-D case. When fast models are required, and especially for estimating discharges, simplifications of model equations (e.g.,

Muskingum-Cunge routing) may be implemented for the whole basin or for only part of it, for which kinematic routings are usually sufficient (David et al., 2015; Follum et al., 2017; Getirana, Peters-Lidard, et al., 2017; Paiva et al., 2013). An optimum setup is likely related to a 1-D-2-D coupling strategy (Andreadis et al., 2017; Hoch, Neal, et al., 2017; Hodges, 2013), for example, the hybrid model systems used to represent river-lake modeling systems (Dargahi & Setegn, 2011; Li et al., 2014; Lopes et al., 2018; Munar et al., 2018; Tanaka et al., 2018; Zhang et al., 2017), and adaptive model meshes are also promising (Hoch, Haag, et al., 2017). In the case of the Negro basin, a 1-D river-floodplain simulation could be performed for most of the basin and 2-D mainly for the interfluvial wetlands and the large floodplains around Negro mainstem (in the case that other output variables than discharge are required). A mixed 1-D/2-D model capability has already been developed for simulating regional areas at coarse scale, including LISFLOOD-FP subgrid model to deal with subgrid floodplain channels (Neal et al., 2012; Schumann et al., 2016), the MGB lateral connections scheme (Fleischmann et al., 2018; Pontes et al., 2017), the CaMa-Flood bifurcation scheme (Ikeuchi et al., 2015; Mateo et al., 2017; Yamazaki, Sato, et al., 2014), and the SIRIPLAN model for the Pantanal wetlands (da Paz et al., 2011). In all these approaches, however, the subgrid parameterization poses important challenges as discussed previously, for example, definition of floodplain flow among neighbor cells. We finally stress that model intercomparison projects are paramount to guide the selection of model dimensionality, including different model structures and case studies, and that new frameworks to compare large-scale hydraulic models are required, especially when considering models at different spatial resolutions and with different model structures (e.g., subgrid parameterization) (Hoch & Trigg, 2018).

Regarding simulated processes, the MGB model is focused on surface water dynamics modeling, while soil and groundwater processes are simulated with simpler strategies. The rainfall-runoff module represents a bucket, single soil layer model, and a multilayer scheme could improve wetlands subjected to dry periods as the interfluvial wetlands. Moving toward integrated surface-groundwater hydrosystems at regional/continental scales is fundamental (Frappart et al., 2019), for example, with lateral groundwater fluxes and stream-aquifer interactions (Flipo et al., 2014; Miguez-Macho & Fan, 2012). Although MGB simplistically simulates the different water table level conditions in the simplified bucket approach within a given model cell, more studies should be performed to understand the extent to which groundwater level interacts with the interfluvial wetlands to maintain their flood levels. On the other hand, earth system models should also include hydrodynamic routings in their frameworks (Zhao et al., 2017). Finally, this study analyzed a coupled hydrologic-hydrodynamic model with calibrated rainfall-runoff parameters. It has been showed even for the continental scale that it is now feasible to satisfactorily calibrate rainfall-runoff parameters to force hydrodynamic models (Siqueira et al., 2018), and it should be pursued by current hydrologic-hydrodynamic models in order to ultimately provide the necessary flow peak estimates (Grimaldi et al., 2019).

Finally, effective parameters in large-scale models should be estimated by aiming at reach-scale estimates with more local relevance (Fleischmann et al., 2019) and considering meaningful hydraulic information (Garambois & Monnier, 2015) by, for example, understanding the river hydraulic visibility and considering remote sensing data sets and location of hydraulic controls for drainage segmentation (Frasson et al., 2017; Garambois et al., 2017; Montazem et al., 2019). Previous regional-scale studies have adopted simplified empirical hydraulic geometry relationships for estimating channel width and depth (Beighley et al., 2009; Coe et al., 2008; Decharme et al., 2008, 2012; Häfliger et al., 2015; Luo et al., 2017; Neal et al., 2012; Paiva et al., 2013; Siqueira et al., 2018; Yamazaki et al., 2012), but distributed parameter values are required, especially for channel cross sections (Fleischmann et al., 2019; Grimaldi et al., 2018; Neal et al., 2015; Tuozzolo et al., 2019). There are now ways of estimating cross sections from remote sensing data (Domeneghetti, 2016; Garambois & Monnier, 2015; Grimaldi et al., 2018), especially in the context of the forthcoming SWOT mission (Biancamaria et al., 2016).

5. Conclusions

This study presents a comparison between 1-D and 2-D regional-scale, fully coupled hydrologic-hydrodynamic models for an entire large river basin with extensive wetlands, and its relevance relies on the fact that most previous evaluations of hydraulic model dimensionalities were performed for local/reach scales only. Conclusions of this study are as follows:

- Both 1-D and 2-D models can provide similar discharge, water levels, and flood extent and volume for large rivers, especially considering parameter uncertainty;
- Regional 1-D and 2-D hydrodynamic models do not provide similar results for complex interfluvial wetlands, where the accurate representation of the diffuse flow pattern and local drainage processes and distributaries is fundamental. In this case 2-D models are preferable;
- The 2-D model generally led to more connectivity among cells and thus facilitated water drainage throughout the basin;
- Model calibration of 1-D or 2-D models can lead to similar discharge and water surface elevation results; however, effective parameter values (e.g., bankfull width and depth and Manning roughness) may be out of the realistic parameter ranges expected at local scales. In this study, the adopted parameter values were parsimoniously kept within realistic ranges;
- A sensitivity test indicated that the 1-D model has an overall larger sensitivity to hydrodynamic parameters for discharge and flood extent but not for water levels; and
- The coupling between hydrologic and hydrodynamic processes is less important than differences in hydrodynamic model dimensionality and parameter uncertainty in the case study (Negro basin, a major tributary of the Amazon).

Such comparison studies are fundamental to foster better understanding of current regional-scale models and to provide important insights for guiding future model developments, especially in the context of future remote sensing observations capabilities and improved computational capacity. Especially, given SWOT and other high-resolution remote sensing data that are arising for estimating hydrodynamic parameters, there is a great opportunity to improve regional-scale models toward hyperresolution and more detailed process representation.

Conflict of Interest

There are no conflicts of interest in this study.

Data Availability Statement

The validation data used in this study are available in the following websites: http://www.estellus.fr/ (GIEMS-D3), https://drive.google.com/drive/folders/1SMbdBZV9gxXd9s3UydLbvuJVftB-SPUB?usp=sharing (SWAF-HR), http://hydroweb.theia-land.fr/ (satellite altimetry), and http://www.snirh.gov.br/hidroweb/ (in situ discharges and water levels), and their main references are cited in the text. MGB model code is available in <https://www.ufrgs.br/lsh/pagina-exemplo-2/mgb-iph-downloads/mgb-4-1/>, and the model input data used in this study are available in <https://drive.google.com/open?id=1A_Y4DmPDVADey-1ufBi8Sz_YQE02buYO>.

Acknowledgments

The first author would like to thank CNPq for funding this research under the Grant Number 141161/2017-5. This study was carried out within the SWOT-MOD, SELECAO, and TOSCA-SOLE projects (https://swot.jpl.nasa.gov/st_projects.htm) of the Surface Water and Ocean Topography (SWOT) Science Team. We also thank the Associate Editor Mário J. Franca and three anonymous reviewers for valuable comments on the manuscript.

References

Aires, F., Miolane, L., Prigent, C., Pham, B., Fluet-Chouinard, E., Lehner, B., et al. (2017). A global dynamic long-term inundation extent dataset at high spatial resolution derived through downscaling of satellite observations. *Journal of Hydrometeorology*, *18*(5), 1305–1325. https://doi.org/10.1175/JHM-D-16-0155.1

Aires, F., Prigent, C., Fluet-Chouinard, E., Yamazaki, D., Papa, F., & Lehner, B. (2018). Comparison of visible and multi-satellite global inundation datasets at high-spatial resolution. *Remote Sensing of Environment*, *216*(July 2017), 427–441. https://doi.org/10.1016/j.rse.2018.06.015

Al Bitar, A., Mialon, A., Kerr, Y. H., Cabot, F., Richaume, P., Jacquette, E., et al. (2017). The global SMOS Level 3 daily soil moisture and brightness temperature maps. *Earth System Science Data*, *9*(1), 293–315. https://doi.org/10.5194/essd-9-293-2017

Alfieri, L., Salamon, P., Bianchi, A., Neal, J., Bates, P., & Feyen, L. (2013). Advances in pan-European flood hazard mapping. *Hydrological Processes*, *28*(13), 4067–4077. https://doi.org/10.1002/hyp.9947

Alho, P., & Aaltonen, J. (2008). Comparing a 1D hydraulic model with a 2D hydraulic model for the simulation of extreme glacial outburst floods. *Hydrological Processes*, *22*(10), 1537–1547. https://doi.org/10.1002/hyp.6692

Allen, G. H., & Pavelsky, T. M. (2018). Global extent of rivers and streams. *Science*, *361*(6402), 585–588. https://doi.org/10.1126/science.aat0636

Alsdorf, D., Bates, P., Melack, J., Wilson, M., & Dunne, T. (2007). Spatial and temporal complexity of the Amazon flood measured from space. *Geophysical Research Letters*, *34*, L08402. https://doi.org/10.1029/2007GL029447

Alsdorf, D. E. (2003). Water storage of the Central Amazon floodplain measured with GIS and remote sensing imagery. *Maintenance*, *93*(1), 55–66. https://doi.org/10.1111/1467-8306.93105

Altenau, E. H., Pavelsky, T. M., Bates, P. D., & Neal, J. C. (2017). The effects of spatial resolution and dimensionality on modeling regional-scale hydraulics in a multichannel river. *Water Resources Research*, *53*, 1683–1701. https://doi.org/10.1002/2016WR019396

Andreadis, K. M., Schumann, G. J. P., Stampoulis, D., Bates, P. D., Brakenridge, G. R., & Kettner, A. J. (2017). Can atmospheric reanalysis data sets be used to reproduce flooding over large scales? *Geophysical Research Letters*, *44*, 10,369–10,377. https://doi.org/10.1002/2017GL075502

Bates, P. D., Horritt, M. S., & Fewtrell, T. J. (2010). A simple inertial formulation of the shallow water equations for efficient two-dimensional flood inundation modelling. *Journal of Hydrology*, *387*(1–2), 33–45. https://doi.org/10.1016/j.jhydrol.2010.03.027

Bates, P. D., Neal, J., Sampson, C., Smith, A., & Trigg, M. (2018). Progress toward hyperresolution models of global flood hazard. In *Risk Modeling for Hazards and Disasters* (pp. 211–232). Oxford, UK: Elsevier.

Bauer, P., Gumbricht, T., & Kinzelbach, W. (2006). A regional coupled surface water/groundwater model of the Okavango Delta, Botswana. *Water Resources Research*, *42*(55). https://doi.org/10.1029/2005WR004234

Beighley, R. E., Eggert, K. G., Dunne, T., He, Y., Gummadi, V., & Verdin, K. L. (2009). Simulating hydrologic and hydraulic processes throughout the Amazon River basin. *Hydrological Processes*, *23*(8), 1221–1235. https://doi.org/10.1002/hyp.7252

Belger, L., Forsberg, B. R., & Melack, J. M. (2011). Carbon dioxide and methane emissions from interfluvial wetlands in the upper Negro River basin, Brazil. *Biogeochemistry*, *105*(1–3), 171–183. https://doi.org/10.1007/s10533-010-9536-0

Bermúdez, M., Neal, J. C., Bates, P. D., Coxon, G., Freer, J. E., Cea, L., et al. (2017). Quantifying local rainfall dynamics and uncertain boundary conditions into a nested regional-local flood modeling system. *Water Resources Research*, *53*, 2770–2785. https://doi.org/10.1002/2016WR019903

Biancamaria, S., Bates, P. D., Boone, A., & Mognard, N. M. (2009). Large-scale coupled hydrologic and hydraulic modelling of the Ob River in Siberia. *Journal of Hydrology*, *379*(1–2), 136–150. https://doi.org/10.1016/j.jhydrol.2009.09.054

Biancamaria, S., Lettenmaier, D. P., & Pavelsky, T. M. (2016). The SWOT Mission and its capabilities for land hydrology. *Surveys in Geophysics*, *37*(2), 307–337. https://doi.org/10.1007/s10712-015-9346-y

Bierkens, M. F. P., Bell, V. A., Burek, P., Chaney, N., Condon, L. E., David, C. H., et al. (2015). Hyper-resolution global hydrological modelling: What is next?. *Hydrological Processes*, *29*(2), 310–320. https://doi.org/10.1002/hyp.10391

Borma, L. S., Da Rocha, H. R., Cabral, O. M., Von Randow, C., Collicchio, E., Kurzatkowski, D., et al. (2009). Atmosphere and hydrological controls of the evapotranspiration over a floodplain forest in the Bananal Island region, Amazonia. *Journal of Geophysical Research*, *114*, G01003. https://doi.org/10.1029/2007JG000641

Cao, N., Lee, H., Jung, H. C., & Yu, H. (2018). Estimation of water level changes of large-scale Amazon wetlands using ALOS2 ScanSAR differential interferometry. *Remote Sensing*, *10*(6). https://doi.org/10.3390/rs10060966

Casulli, V., & Stelling, G. S. (2011). Semi-implicit subgrid modelling of three-dimensional free-surface flows. *International Journal for Numerical Methods in Fluids*, *67*(4), 441–449. https://doi.org/10.1002/fld.2361

Chatterjee, C., Förster, S., & Bronstert, A. (2008). Comparison of hydrodynamic models of different complexities to model floods with emergency storage areas. *Hydrological Processes*, *22*(24), 4695–4709. https://doi.org/10.1002/hyp.7079

Chen, S., Garambois, P. A., Finaud-Guyot, P., Dellinger, G., Mosé, R., Terfous, A., et al. (2018). Variance based sensitivity analysis of 1D and 2D hydraulic models: An experimental urban flood case. *Environmental Modelling and Software*, *109*(August), 167–181. https://doi.org/10.1016/j.envsoft.2018.08.008

Coe, M. T., Costa, M. H., & Howard, E. A. (2008). Simulating the surface waters of the Amazon River basin: Impacts of new river geomorphic and flow parameterizations. *Hydrological Processes*, *22*(14), 2542–2553. https://doi.org/10.1002/hyp.6850

Collischonn, W., Allasia, D., da Silva, B. C., & Tucci, C. E. M. (2007). The MGB-IPH model for large-scale rainfall-runoff modelling. *Hydrological Sciences Journal*, *52*(5), 878–895. https://doi.org/10.1623/hysj.52.5.878

Cook, A., & Merwade, V. (2009). Effect of topographic data, geometric configuration and modeling approach on flood inundation mapping. *Journal of Hydrology*, *377*(1–2), 131–142. https://doi.org/10.1016/j.jhydrol.2009.08.015

Czuba, J. A., David, S. R., Edmonds, D. A., & Ward, A. S. (2019). Dynamics of surface-water connectivity in a low-gradient meandering river floodplain. *Water Resources Research*, *55*, 1849–1870. https://doi.org/10.1029/2018WR023527

Da Paz, A. R., Collischonn, W., Bravo, J. M., Bates, P. D., & Baugh, C. (2014). The influence of vertical water balance on modelling Pantanal (Brazil) spatio-temporal inundation dynamics. *Hydrological Processes*, *28*(10), 3539–3553. https://doi.org/10.1002/hyp.9897

da Paz, A. R., Collischonn, W., Tucci, C. E. M., & Padovani, C. R. (2011). Large-scale modelling of channel flow and floodplain inundation dynamics and its application to the Pantanal (Brazil). *Hydrological Processes*, *25*(9), 1498–1516. https://doi.org/10.1002/hyp.7926

Dargahi, B., & Setegn, S. G. (2011). Combined 3D hydrodynamic and watershed modelling of Lake Tana, Ethiopia. *Journal of Hydrology*, *398*(1–2), 44–64. https://doi.org/10.1016/j.jhydrol.2010.12.009

David, C. H., Famiglietti, J. S., Yang, Z.-L., & Eijkhout, V. (2015). Enhanced fixed-size parallel speedup with the Muskingum method using a trans-boundary approach and a large subbasins approximation. *Water Resources Research*, *51*, 7547–7571. https://doi.org/10.1002/2014WR016650

David, C. H., Hobbs, J. M., Turmon, M. J., Emery, C. M., Reager, J. T., & Famiglietti, J. S. (2019). Analytical propagation of runoff uncertainty into discharge uncertainty through a large river network. *Geophysical Research Letters*, *46*(14). https://doi.org/10.1029/2019GL083342

Decharme, B., Alkama, R., Papa, F., Faroux, S., Douville, H., & Prigent, C. (2012). Global off-line evaluation of the ISBA-TRIP flood model. *Climate Dynamics*, *38*(7–8), 1389–1412. https://doi.org/10.1007/s00382-011-1054-9

Decharme, B., Douville, H., Prigent, C., Papa, F., & Aires, F. (2008). A new river flooding scheme for global climate applications: Off-line evaluation over South America. *Journal of Geophysical Research*, *113*, D11110. https://doi.org/10.1029/2007JD009376

Dimitriadis, P., Tegos, A., Oikonomou, A., Pagana, V., Koukouvinos, A., Mamassis, N., et al. (2016). Comparative evaluation of 1D and quasi-2D hydraulic models based on benchmark and real-world applications for uncertainty assessment in flood mapping. *Journal of Hydrology*, *534*, 478–492. https://doi.org/10.1016/j.jhydrol.2016.01.020

Domeneghetti, A. (2016). On the use of SRTM and altimetry data for flood modeling in data-sparse regions. *Water Resources Research*, *52*, 2901–2918. https://doi.org/10.1002/2015WR017967

Dottori, F., Di Baldassarre, G., & Todini, E. (2013). Detailed data is welcome, but with a pinch of salt: Accuracy, precision, and uncertainty in flood inundation modeling. *Water Resources Research*, *49*, 6079–6085. https://doi.org/10.1002/wrcr.20406

Dottori, F., & Todini, E. (2013). Testing a simple 2D hydraulic model in an urban flood experiment. *Hydrological Processes*, *27*(9), 1301–1320. https://doi.org/10.1002/hyp.9370

Dottori, F., Salamon, P., Bianchi, A., Alfieri, L., Hirpa, F. A., & Feyen, L. (2016). Development and evaluation of a framework for global flood hazard mapping. *Advances in Water Resources*, *94*, 87–102. https://doi.org/10.1016/j.advwatres.2016.05.002

Esri (2009). *World imagery*, Redlands, CA: ESRI (Environmental Systems Research Institute). Retrieved June 12, 2019, from https://www.arcgis.com/home/item.html?id=10df2279f9684e4a9f6a7f08febac2a9

Falter, D., Dung, N. V., Vorogushyn, S., Schröter, K., Hundecha, Y., Kreibich, H., et al. (2016). Continuous, large-scale simulation model for flood risk assessments: Proof-of-concept. *Journal of Flood Risk Management*, *9*(1), 3–21. https://doi.org/10.1111/jfr3.12105

Fan, F., Buarque, D. C., Pontes, P. R. M., & Collischonn, W. (2015). Um mapa de unidades de resposta hidrológica para a América do Sul. In *Anais do XXI Simpósio Brasileiro de Recursos Hídricos* (pp. 1–8). Brasília: ABRH.

Fleischmann, A., Paiva, R., & Collischonn, W. (2019). Can regional to continental river hydrodynamic models be locally relevant? A cross-scale comparison. *Journal of Hydrology X*, *3*, 100,027–100,045. https://doi.org/10.1016/j.hydroa.2019.100027

Fleischmann, A., Siqueira, V., Paris, A., Collischonn, W., Paiva, R., Pontes, P., et al. (2018). Modelling hydrologic and hydrodynamic processes in basins with large semi-arid wetlands. *Journal of Hydrology*, *561*(August 2017), 943–959. https://doi.org/10.1016/j.jhydrol.2018.04.041

Flipo, N., Mouhri, A., Labarthe, B., Biancamaria, S., Rivière, A., & Weill, P. (2014). Continental hydrosystem modelling: The concept of nested stream-aquifer interfaces. *Hydrology and Earth System Sciences*, *18*(8), 3121–3149. https://doi.org/10.5194/hess-18-3121-2014

Follum, M. L., Tavakoly, A. A., Niemann, J. D., & Snow, A. D. (2017). AutoRAPID: A model for prompt streamflow estimation and flood inundation mapping over regional to continental extents. *Journal of the American Water Resources Association*, *53*(2), 280–299. https://doi.org/10.1111/1752-1688.12476

Frappart, F., Papa, F., Famiglietti, J. S., Prigent, C., Rossow, W. B., & Seyler, F. (2008). Interannual variations of river water storage from a multiple satellite approach: A case study for the Rio Negro River basin. *Journal of Geophysical Research*, *113*, D21104. https://doi.org/10.1029/2007JD009438

Frappart, F., Papa, F., Güntner, A., Tomasella, J., Pfeffer, J., Ramillien, G., et al. (2019). The spatio-temporal variability of groundwater storage in the Amazon River basin. *Advances in Water Resources*, *124*(December 2018), 41–52. https://doi.org/10.1016/j.advwatres.2018.12.005

Frappart, F., Papa, F., Malbeteau, Y., León, J., Ramillien, G., Prigent, C., et al. (2014). Surface freshwater storage variations in the Orinoco floodplains using multi-satellite observations. *Remote Sensing*, *7*(1), 89–110. https://doi.org/10.3390/rs70100089

Frappart, F., Papa, F., Santos Da Silva, J., Ramillien, G., Prigent, C., Seyler, F., & Calmant, S. (2012). Surface freshwater storage and dynamics in the Amazon basin during the 2005 exceptional drought. *Environmental Research Letters*, *7*(4), 044010. https://doi.org/10.1088/1748-9326/7/4/044010

Frappart, F., Seyler, F., Martinez, J., León, J. G., & Cazenave, A. (2005). Floodplain water storage in the Negro River basin estimated from microwave remote sensing of inundation area and water levels. *Remote Sensing of Environment*, *99*(4), 387–399. https://doi.org/10.1016/j.rse.2005.08.016

Frasson, R. P. d. M., Pavelsky, T. M., Fonstad, M. A., Durand, M. T., Allen, G. H., Schumann, G., et al. (2019). Global relationships between river width, slope, catchment area, meander wavelength, sinuosity, and discharge. *Geophysical Research Letters*, *46*, 3252–3262. https://doi.org/10.1029/2019GL082027

Frasson, R. P. d. M., Wei, R., Durand, M., Minear, J. T., Domeneghetti, A., Schumann, G., et al. (2017). Automated river reach definition strategies: Applications for the Surface Water and Ocean Topography Mission. *Water Resources Research*, *53*, 8164–8186. https://doi.org/10.1002/2017WR020887

Garambois, P., & Monnier, J. (2015). Inference of effective river properties from remotely sensed observations of water surface. *Advances in Water Resources*, *79*, 103–120. https://doi.org/10.1016/j.advwatres.2015.02.007

Garambois, P. A., Calmant, S., Roux, H., Paris, A., Monnier, J., Finaud-Guyot, P., et al. (2017). Hydraulic visibility: Using satellite altimetry to parameterize a hydraulic model of an ungauged reach of a braided river. *Hydrological Processes*, *31*(4), 756–767. https://doi.org/10.1002/hyp.11033

Getirana, A., Espinoza, J. C. V., Ronchail, J., & Filho, O. C. R. (2011). Assessment of different precipitation datasets and their impacts on the water balance of the Negro River basin. *Journal of Hydrology*, *404*(3–4), 304–322. https://doi.org/10.1016/j.jhydrol.2011.04.037

Getirana, A., Peters-Lidard, C., Rodell, M., & Bates, P. D. (2017). Trade-off between cost and accuracy in large-scale surface water dynamic modeling. *Water Resources Research*, *53*, 4942–4955. https://doi.org/10.1002/2017WR020519

Getirana, A., Kumar, S., Girotto, M., & Rodell, M. (2017). Rivers and floodplains as key components of global terrestrial water storage variability. *Geophysical Research Letters*, *44*, 10,359–10,368. https://doi.org/10.1002/2017GL074684

Grimaldi, S., Li, Y., Walker, J. P., & Pauwels, V. R. N. (2018). Effective representation of river geometry in hydraulic flood forecast models. *Water Resources Research*, *54*, 1031–1057. https://doi.org/10.1002/2017WR021765

Grimaldi, S., Schumann, G. J. -P., Shokri, A., Walker, J. P., & Pauwels, V. R. N. (2019). Challenges, opportunities and pitfalls for global coupled hydrologic-hydraulic modeling of floods. *Water Resources Research*, *55*, 5277–5300. https://doi.org/10.1029/2018WR024289

Guimarães, F., & Bueno, G. (2016). As campinas e campinaranas amazônicas. *Caderno de Geografia*, *26*(45), 113–133. https://doi.org/10.5752/p.2318-2962.2016v26n.45p.113

Häfliger, V., Martin, E., Boone, A., Habets, F., David, C. H., Garambois, P.-A., et al. (2015). Evaluation of regional-scale river depth simulations using various routing schemes within a hydrometeorological modeling framework for the preparation of the SWOT Mission. *Journal of Hydrometeorology*, *16*(4), 1821–1842. https://doi.org/10.1175/JHM-D-14-0107.1

Hamilton, S. K., Sippel, S. J., & Melack, J. M. (2002). Comparison of inundation patterns among major South American floodplains. *Journal of Geophysical Research*, *107*(127), pp.LBA-5. https://doi.org/10.1029/2000jd000306

Hess, L. L., Melack, J. M., Affonso, A. G., Barbosa, C., Gastil-buhl, M., & Novo, E. M. L. M. (2015). Wetlands of the lowland Amazon basin: Extent, vegetative cover, and dual-season inundated area as mapped with JERS-1 synthetic aperture radar. *Wetlands*, *35*(4), 745–756. https://doi.org/10.1007/s13157-015-0666-y

Hirabayashi, Y., Mahendran, R., Koirala, S., Konoshima, L., Yamazaki, D., Watanabe, S., et al. (2013). Global flood risk under climate change. *Nature Climate Change*, *3*(9), 816–821. https://doi.org/10.1038/nclimate1911

Hoch, J. M., Haag, A. V., Van Dam, A., Winsemius, H. C., Van Beek, L. P. H., & Bierkens, M. F. P. (2017). Assessing the impact of hydrodynamics on large-scale flood wave propagation: A case study for the Amazon basin. *Hydrology and Earth System Sciences*, *21*(1), 117–132. https://doi.org/10.5194/hess-21-117-2017

Hoch, J., & Trigg, M. A. (2018). Advancing global flood hazard simulations by improving comparability, benchmarking, and integration of global flood models. *Environmental Research Letters*. https://doi.org/10.1088/1748-9326/aaf3d3

Hoch, J. M., Neal, J. C., Baart, F., Van Beek, R., Winsemius, H. C., Bates, P. D., & Bierkens, M. F. P. (2017). GLOFRIM v1.0-A globally applicable computational framework for integrated hydrological-hydrodynamic modelling. *Geoscientific Model Development*, *10*(10), 3913–3929. https://doi.org/10.5194/gmd-10-3913-2017

Hodges, B. R. (2013). Challenges in continental river dynamics. *Environmental Modelling and Software*, *50*, 16–20. https://doi.org/10.1016/j.envsoft.2013.08.010

Horritt, M. S., & Bates, P. D. (2002). Evaluation of 1D and 2D numerical models for predicting river flood inundation. *Journal of Hydrology*, *268*(1–4), 87–99. https://doi.org/10.1016/S0022-1694(02)00121-X

Huffman, G., Bolvin, D., Nelkin, E., Wolff, D., Adler, R., Gu, G., et al. (2007). The TRMM Multisatellite Precipitation Analysis (TMPA) quasi-global, multiyear, combined-sensor precipitation estimates at fine scales. *Journal of Hydrometeorology*, *8*(1), 38–55. https://doi.org/10.1175/JHM560.1

Hunter, N. M., Bates, P. D., Horritt, M. S., & Wilson, M. D. (2007). Simple spatially-distributed models for predicting flood inundation: A review. *Geomorphology*, *90*(3–4), 208–225. https://doi.org/10.1016/j.geomorph.2006.10.021

Ikeuchi, H., Hirabayashi, Y., Yamazaki, D., Kiguchi, M., Koirala, S., Nagano, T., et al. (2015). Modeling complex flow dynamics of fluvial floods exacerbated by sea level rise in the Ganges-Brahmaputra-Meghna Delta. *Environmental Research Letters*, *10*(12), 124011. https://doi.org/10.1088/1748-9326/10/12/124011

Jung, H. C., Hamski, J., Durand, M., Alsdorf, D., Hossain, F., Lee, H., et al. (2010). Characterization of complex fluvial systems using remote sensing of spatial and temporal water level variations in the Amazon, Congo, and Brahmaputra Rivers. *Earth Surface Processes and Landforms*, *35*(3), 294–304. https://doi.org/10.1002/esp.1914

Junk, W. J., Piedade, M. T. F., Schöngart, J., Cohn-Haft, M., Adeney, J. M., & Wittmann, F. (2011). A classification of major naturally-occurring Amazonian lowland wetlands. *Wetlands*, *31*(4), 623–640. https://doi.org/10.1007/s13157-011-0190-7

Kauffeldt, A., Wetterhall, F., Pappenberger, F., Salamon, P., & Thielen, J. (2016). Technical review of large-scale hydrological models for implementation in operational flood forecasting schemes on continental level. *Environmental Modelling and Software*, *75*, 68–76. https://doi.org/10.1016/j.envsoft.2015.09.009

Kerr, Y. H., Waldteufel, P., Wigneron, J. P., Martinuzzi, J. M., Font, J., & Berger, M. (2001). Soil moisture retrieval from space: The Soil Moisture and Ocean Salinity (SMOS) mission. *IEEE Transactions on Geoscience and Remote Sensing*, *39*(8), 1729–1735. https://doi.org/10.1109/36.942551

Kim, D., Lee, H., Laraque, A., Tshimanga, R. M., Yuan, T., Jung, H. C., et al. (2017). Mapping spatio-temporal water level variations over the central Congo River using PALSAR ScanSAR and Envisat altimetry data. *International Journal of Remote Sensing*, *38*(23), 7021–7040. https://doi.org/10.1080/01431161.2017.1371867

Latrubesse, E. M., Arima, E. Y., Dunne, T., Park, E., Baker, V. R., D'Horta, F. M., et al. (2017). Damming the rivers of the Amazon basin. *Nature*, *546*(7658), 363–369. https://doi.org/10.1038/nature22333

Latrubesse, E. M., & Franzinelli, E. (2005). The late Quaternary evolution of the Negro River, Amazon, Brazil: Implications for island and floodplain formation in large anabranching tropical systems. *Geomorphology*, *70*(3–4), 372–397. https://doi.org/10.1016/j.geomorph.2005.02.014

Latrubesse, E. M., & Stevaux, J. C. (2015). The Anavilhanas and Mariuá archipelagos: Fluvial wonders from the Negro River, Amazon basin. In B. C. Vieira, A. A. R. Salgado, & L. J. C. Santos (Eds.), *Choice reviews online* (Vol. 53, pp. 157–169). Dordrecht: Springer Netherlands.

Lehner, B., Verdin, K., & Jarvis, A. (2008). New global hydrography derived from spaceborne elevation data. *Eos*, *89*(10), 93. https://doi.org/10.1029/2008EO100001

Li, Y., Zhang, Q., Yao, J., Werner, A. D., & Li, X. (2014). Hydrodynamic and hydrological modeling of the Poyang Lake catchment system in China. *Journal of Hydrologic Engineering*, *19*(3), 607–616. https://doi.org/10.1061/(ASCE)HE.1943-5584.0000835

Liu, Y., Weerts, A. H., Clark, M., Hendricks Franssen, H. J., Kumar, S., Moradkhani, H., et al. (2012). Advancing data assimilation in operational hydrologic forecasting: Progresses, challenges, and emerging opportunities. *Hydrology and Earth System Sciences*, *16*(10), 3863–3887. https://doi.org/10.5194/hess-16-3863-2012

Lopes, V. A. R., Fan, F. M., Pontes, P. R. M., Siqueira, V. A., Collischonn, W., & da Motta Marques, D. (2018). A first integrated modelling of a river-lagoon large-scale hydrological system for forecasting purposes. *Journal of Hydrology*, *565*, 177–196. https://doi.org/10.1016/j.jhydrol.2018.08.011

Luo, X., Li, H.-Y., Leung, L. R., Tesfa, T. K., Getirana, A., Papa, F., & Hess, L. L. (2017). Modeling surface water dynamics in the Amazon basin using MOSART-inundation v1.0: Impacts of geomorphological parameters and river flow representation. *Geoscientific Model Development*, *10*(3), 1233–1259. https://doi.org/10.5194/gmd-10-1233-2017

Mateo, R. C., Yamazaki, D., Kim, H., Champathong, A., Vaze, J., & Oki, T. (2017). Impacts of spatial resolution and representation of flow connectivity on large-scale simulation of floods. *Hydrology and Earth System Sciences*, *21*(10), 5143–5163. https://doi.org/10.5194/hess-21-5143-2017

Meade, R. H., Rayol, J. M., da Conceição, S. C., & Natividade, J. R. G. (1991). Backwater effects in the Amazon River of basin. *Environmental Geology and Water Sciences*, *18*(2), 105–114. https://doi.org/10.1007/BF01704664

Mejia, A. I., & Reed, S. M. (2011). Evaluating the effects of parameterized cross section shapes and simplified routing with a coupled distributed hydrologic and hydraulic model. *Journal of Hydrology*, *409*(1–2), 512–524. https://doi.org/10.1016/j.jhydrol.2011.08.050

Melack, J. M., & Hess, L. L. (2010). Remote sensing of the distribution and extent of wetlands in the Amazon basin. In *Amazonian Floodplain Forests*, *Ecological Studies (Analysis and Synthesis)* (Vol. 210, pp. 43–59). Dordrecht: Springer.

Miguez-Macho, G., & Fan, Y. (2012). The role of groundwater in the Amazon water cycle: 1. Influence on seasonal streamflow, flooding and wetlands. *Journal of Geophysical Research*, *117*, D15113. https://doi.org/10.1029/2012JD017539

Montazem, A., Garambois, P., Calmant, S., Finaud-Guyot, P., Monnier, J., Medeiros Moreira, D., et al. (2019). Wavelet-based river segmentation using hydraulic control-preserving water surface elevation profile properties. *Geophysical Research Letters*, *46*, 6534–6543. https://doi.org/10.1029/2019GL082986

Montero, J. C., & Latrubesse, E. M. (2013). The igapó of the Negro River in central Amazonia: Linking late-successional inundation forest with fluvial geomorphology. *Journal of South American Earth Sciences*, *46*, 137–149. https://doi.org/10.1016/j.jsames.2013.05.009

Munar, A. M., Cavalcanti, J. R., Bravo, J. M., Fan, F. M., da Motta-Marques, D., & Fragoso, C. R. (2018). Coupling large-scale hydrological and hydrodynamic modeling: Toward a better comprehension of watershed-shallow lake processes. *Journal of Hydrology*, *564*(March), 424–441. https://doi.org/10.1016/j.jhydrol.2018.07.045

Neal, J., Schumann, G., & Bates, P. (2012). A subgrid channel model for simulating river hydraulics and floodplain inundation over large and data sparse areas. *Water Resources Research*, *48*, W11506. https://doi.org/10.1029/2012WR012514

Neal, J. C., Odoni, N. A., Trigg, M. A., Freer, J. E., Garcia-Pintado, J., Mason, D. C., et al. (2015). Efficient incorporation of channel cross-section geometry uncertainty into regional and global scale flood inundation models. *Journal of Hydrology*, *529*, 169–183. https://doi.org/10.1016/j.jhydrol.2015.07.026

New, M., Lister, D., Hulme, M., & Makin, I. (2002). A high-resolution data set of surface climate over global land areas. *Climate Research*, *21*, 1–25. https://doi.org/10.3354/cr021001

O'Loughlin, F., Trigg, M. A., Schumann, G. J. P., & Bates, P. D. (2013). Hydraulic characterization of the middle reach of the Congo River. *Water Resources Research*, *49*, 5059–5070. https://doi.org/10.1002/wrcr.20398

O'Loughlin, F. E., Neal, J., Schumann, G. J. P., Beighley, E., & Bates, P. D. (2020). A LISFLOOD-FP hydraulic model of the middle reach of the Congo. *Journal of Hydrology*, *580*(May 2019), 124203. https://doi.org/10.1016/j.jhydrol.2019.124203

Paiva, R., Buarque, D. C., Collischonn, W., Bonnet, M. P., Frappart, F., Calmant, S., & Bulhões Mendes, C. A. (2013). Large-scale hydrologic and hydrodynamic modeling of the Amazon River basin. *Water Resources Research*, *49*, 1226–1243. https://doi.org/10.1002/wrcr.20067

Paiva, R. C. D., Collischonn, W., & Tucci, C. E. M. (2011). Large scale hydrologic and hydrodynamic modeling using limited data and a GIS based approach. *Journal of Hydrology*, *406*(3–4), 170–181. https://doi.org/10.1016/j.jhydrol.2011.06.007

Papa, F., Frappart, F., Güntner, A., Prigent, C., Aires, F., Getirana, A. C. V., & Maurer, R. (2013). Surface freshwater storage and variability in the Amazon basin from multi-satellite observations, 1993–2007. *Journal of Geophysical Research: Atmospheres*, *118*, 11,951–11,965. https://doi.org/10.1002/2013JD020500

Papa, F., Prigent, C., Aires, F., Jimenez, C., Rossow, W. B., & Matthews, E. (2010). Interannual variability of surface water extent at the global scale, 1993–2004. *Journal of Geophysical Research*, *115*, D12111. https://doi.org/10.1029/2009JD012674

Pappenberger, F., Dutra, E., Wetterhall, F., & Cloke, H. L. (2012). Deriving global flood hazard maps of fluvial floods through a physical model cascade. *Hydrology and Earth System Sciences*, *16*(11), 4143–4156. https://doi.org/10.5194/hess-16-4143-2012

Park, E., & Latrubesse, E. M. (2017). The hydro-geomorphologic complexity of the lower Amazon River floodplain and hydrological connectivity assessed by remote sensing and field control. *Remote Sensing of Environment*, *198*, 321–332. https://doi.org/10.1016/j.rse.2017.06.021

Parrens, M., Al Bitar, A., Frappart, F., Paiva, R., Wongchuig, S., Papa, F., et al. (2019). High resolution mapping of inundation area in the Amazon basin from a combination of L-band passive microwave, optical and radar datasets. *International Journal of Applied Earth Observation and Geoinformation*, *81*, 58–71. https://doi.org/10.1016/j.jag.2019.04.011

Parrens, M., Al Bitar, A., Frappart, F., Papa, F., Calmant, S., Crétaux, J.-F., et al. (2017). Mapping dynamic water fraction under the tropical rain forests of the Amazonian basin from SMOS brightness temperatures. *Water*, *9*(5), 350. https://doi.org/10.3390/w9050350

Paz, A. R., & Collischonn, W. (2007). River reach length and slope estimates for large-scale hydrological models based on a relatively high-resolution digital elevation model. *Journal of Hydrology*, *343*(3–4), 127–139. https://doi.org/10.1016/j.jhydrol.2007.06.006

Paz, A. R., Collischonn, W., & Lopes da Silveira, A. L. (2006). Improvements in large-scale drainage networks derived from digital elevation models. *Water Resources Research*, *42*, e2019WR026812. https://doi.org/10.1029/2005WR004544

Pekel, J., Cottam, A., Gorelick, N., & Belward, A. S. (2016). High-resolution mapping of global surface water and its long-term changes. *Nature*, *540*(7633), 418–422. https://doi.org/10.1038/nature20584

Pianosi, F., Beven, K., Freer, J., Hall, J. W., Rougier, J., Stephenson, D. B., & Wagener, T. (2016). Sensitivity analysis of environmental models: A systematic review with practical workflow. *Environmental Modelling and Software*, *79*, 214–232. https://doi.org/10.1016/j.envsoft.2016.02.008

Pinel, S., Bonnet, M., Da Silva, J., Sampaio, T. C., Garnier, J., Catry, T., et al. (2019). Flooding dynamics within an Amazonian floodplain: Water circulation patterns and inundation duration. *Water Resources Research*, *56*, e2019WR026081. https://doi.org/10.1029/2019WR026081

Pontes, P. R. M., Fan, F. M., Fleischmann, A. S., de Paiva, R. C. D., Buarque, D. C., Siqueira, V. A., et al. (2017). MGB-IPH model for hydrological and hydraulic simulation of large floodplain river systems coupled with open source GIS. *Environmental Modelling and Software*, *94*, 1–20. https://doi.org/10.1016/j.envsoft.2017.03.029

Prigent, C., Papa, F., Aires, F., Rossow, W. B., & Matthews, E. (2007). Global inundation dynamics inferred from multiple satellite observations, 1993-2000. *Journal of Geophysical Research*, *112*, D12113. https://doi.org/10.1029/2006JD007847

Reis, V., Hermoso, V., Hamilton, S. K., Bunn, S. E., Fluet-Chouinard, E., Venables, B., & Linke, S. (2019). Characterizing seasonal dynamics of Amazonian wetlands for conservation and decision making. *Aquatic Conservation: Marine and Freshwater Ecosystems*, *29*. https://doi.org/10.1002/aqc.3051

Rennó, C. D., Nobre, A. D., Cuartas, L. A., Soares, J. V., Hodnett, M. G., Tomasella, J., & Waterloo, M. J. (2008). HAND, a new terrain descriptor using SRTM-DEM: Mapping terra-firme rainforest environments in Amazonia. *Remote Sensing of Environment*, *112*(9), 3469–3481. https://doi.org/10.1016/j.rse.2008.03.018

Revel, M., Ikeshima, D., Yamazaki, D., & Kanae, S. A. (2019). A physically based empirical localization method for assimilating synthetic SWOT observations of a continental-scale river: A case study in the Congo basin. *Water*, *11*(4), 829. https://doi.org/10.3390/w11040829

Rossetti, D. F., Bertani, T. C., Zani, H., Cremon, E. H., & Hayakawa, E. H. (2012). Late Quaternary sedimentary dynamics in Western Amazonia: Implications for the origin of open vegetation/forest contrasts. *Geomorphology*, *177-178*, 74–92. https://doi.org/10.1016/j.geomorph.2012.07.015

Rossetti, D. F., Gribel, R., Rennó, C. D., Cohen, M. C. L., Moulatlet, G. M., Cordeiro, C. L. d. O., & Rodrigues, E. S. d. F. (2017). Late Holocene tectonic influence on hydrology and vegetation patterns in a northern Amazonian megafan. *Catena*, *158*, 121–130. https://doi.org/10.1016/j.catena.2017.06.022

Sampson, C. C., Smith, A. M., Bates, P. D., Neal, J. C., Alfieri, L., & Freer, J. E. (2015). A high-resolution global flood hazard model. *Water Resources Research*, *51*, 7358–7381. https://doi.org/10.1002/2015WR016954

Sanders, B. F., Schubert, J. E., & Gallegos, H. A. (2008). Integral formulation of shallow-water equations with anisotropic porosity for urban flood modeling. *Journal of Hydrology*, *362*(1–2), 19–38. https://doi.org/10.1016/j.jhydrol.2008.08.009

Santos da Silva, J., Calmant, S., Seyler, F., Rotunno Filho, O. C., Cochonneau, G., & Mansur, W. J. (2010). Water levels in the Amazon basin derived from the ERS 2 and ENVISAT radar altimetry missions. *Remote Sensing of Environment*, *114*(10), 2160–2181. https://doi.org/10.1016/j.rse.2010.04.020

Santos, J. O. S., Nelson, B. W., & Giovannini, C. A. (1993). Corpos de areia sob leitos abandonados de grandes rios. *Ciência Hoje*, *16*(93), 22–25.

Schumann, G. J. P., Stampoulis, D., Smith, A. M., Sampson, C. C., Andreadis, K. M., Neal, J. C., & Bates, P. D. (2016). Rethinking flood hazard at the global scale. *Geophysical Research Letters*, *43*, 10,249–10,256. https://doi.org/10.1002/2016GL070260

Schumann, J.-P., Neal, J. C., Voisin, N., Andreadis, K. M., Pappenberger, F., Phanthuwongpakdee, N., et al. (2013). A first large scale flood inundation forecasting model. *Water Resources Research*, *49*, 6248–6257. https://doi.org/10.1002/wrcr.20521

Seyler, F., Muller, F., Cochonneau, G., Guimarães, L., & Guyot, J. L. (2009). Watershed delineation for the Amazon sub-basin system using GTOPO30 DEM and a drainage network extracted from JERS SAR images. *Hydrological Processes*, *23*(22), 3173–3185. https://doi.org/10.1002/hyp.7397

Siqueira, V. A., Paiva, R. C. D., Fleischmann, A. S., Fan, F. M., Ruhoff, A. L., Pontes, P. R. M., et al. (2018). Toward continental hydrologic-hydrodynamic modeling in South America. *Hydrology and Earth System Sciences*, *22*(9), 4815–4842. https://doi.org/10.5194/hess-22-4815-2018

Siqueira, V. A., Fleischmann, A., Jardim, P. F., Fan, F. M., & Collischonn, W. (2016). IPH-hydro tools: A GIS coupled tool for watershed topology acquisition in an open-source environment. *Revista Brasileira de Recursos Hídricos*, *21*(1), 274–287. https://doi.org/10.21168/rbrh.v21n1.p274-287

Sorribas, M. V., Paiva, R. C. D., Melack, J. M., Bravo, J. M., Jones, C., Carvalho, L., et al. (2016). Projections of climate change effects on discharge and inundation in the Amazon basin. *Climatic Change*, *136*(3-4), 555–570. https://doi.org/10.1007/s10584-016-1640-2

Tanaka, T., Yoshioka, H., Siev, S., Fujii, H., Fujihara, Y., Hoshikawa, K., et al. (2018). An integrated hydrological-hydraulic model for simulating surface water flows of a shallow lake surrounded by large floodplains. *Water*, *10*(9), 1213. https://doi.org/10.3390/w10091213

Taylor, C. M. (2010). Feedbacks on convection from an African wetland. *Geophysical Research Letters*, *37*. https://doi.org/10.1029/2009gl041652

Trigg, M. A., Birch, C. E., Neal, J. C., Bates, P. D., Smith, A., Sampson, C. C., et al. (2016). The credibility challenge for global fluvial flood risk analysis. *Environmental Research Letters*, *11*(9). https://doi.org/10.1088/1748-9326/11/9/094014

Trigg, M. A., Wilson, M. D., Bates, P. D., Horritt, M. S., Alsdorf, D. E., Forsberg, B. R., & Vega, M. C. (2009). Amazon flood wave hydraulics. *Journal of Hydrology*, *374*(1–2), 92–105. https://doi.org/10.1016/j.jhydrol.2009.06.004

Tshimanga, R. M., & Hughes, D. A. (2014). Basin-scale performance of a semidistributed rainfall-runoff model for hydrological predictions and water resources assessment of large rivers: The Congo River. *Water Resources Research*, *50*, 1174–1188. https://doi.org/10.1002/2013WR014310

Tuozzolo, S., Langhorst, T., de Moraes Frasson, R. P., Pavelsky, T., & Durand, M. (2019). The impact of reach averaging Manning's equation for an in-situ dataset of water surface elevation, width, and slope. *Journal of Hydrology*, *578*. https://doi.org/10.1016/j.jhydrol.2019.06.038

Bernhofen, M. V., Whyman, C., Trigg, M. A., Sleigh, P. A., Smith, A. M., Sampson, C. C., et al. (2018). A first collective validation of global fluvial flood models for major floods in Nigeria and Mozambique. *Environmental Research Letters*, *13*(10), 104,007. https://doi.org/10.1088/1748-9326/aae014

Wilson, M. D., Bates, P., Alsdorf, D., Forsberg, B., Horritt, M., Melack, J., et al. (2007). Modeling large-scale inundation of Amazonian seasonally flooded wetlands. *Geophysical Research Letters*, *34*, e2019WR026812. https://doi.org/10.1029/2007GL030156

Wing, O. E. J., Bates, P. D., Sampson, C. C., Smith, A. M., Johnson, K. A., & Erickson, T. A. (2017). Validation of a 30 m resolution flood hazard model of the conterminous United States. *Water Resources Research*, *53*, 7968–7986. https://doi.org/10.1002/2017WR020917

Winsemius, H. C., Aerts, J. C. J. H., Van Beek, L. P. H., Bierkens, M. F. P., Bouwman, A., Jongman, B., et al. (2016). Global drivers of future river flood risk. *Nature Climate Change*, *6*(4), 381–385. https://doi.org/10.1038/nclimate2893

Wood, E. F., Roundy, J. K., Troy, T. J., Van Beek, L. P. H., Bierkens, M. F. P., Blyth, E., et al. (2011). Hyperresolution global land surface modeling: Meeting a grand challenge for monitoring Earth's terrestrial water. *Water Resources Research*, *47*, 369. https://doi.org/10.1029/2010WR010090

Yamazaki, D., de Almeida, G. A. M., & Bates, P. D. (2013). Improving computational efficiency in global river models by implementing the local inertial flow equation and a vector-based river network map. *Water Resources Research*, *49*, 7221–7235. https://doi.org/10.1002/wrcr.20552

Yamazaki, D., Ikeshima, D., Tawatari, R., Yamaguchi, T., O'Loughlin, F., Neal, J. C., et al. (2017). A high-accuracy map of global terrain elevations. *Geophysical Research Letters*, *44*, 5844–5853. https://doi.org/10.1002/2017GL072874

Yamazaki, D., Kanae, S., Kim, H., & Oki, T. (2011). A physically based description of floodplain inundation dynamics in a global river routing model. *Water Resources Research*, W04501. https://doi.org/10.1029/2010WR009726

Yamazaki, D., Lee, H., Alsdorf, D. E., Dutra, E., Kim, H., Kanae, S., & Oki, T. (2012). Analysis of the water level dynamics simulated by a global river model: A case study in the Amazon River. *Water Resources Research*, *48*, W09508. https://doi.org/10.1029/2012WR011869

Yamazaki, D., O'Loughlin, F., Trigg, M. A., Miller, Z. F., Pavelsky, T. M., & Bates, P. D. (2014). Development of the global width database for large rivers. *Water Resources Research*, *50*, 3467–3480. https://doi.org/10.1002/2013WR014664

Yamazaki, D., Sato, T., Kanae, S., Hirabayashi, Y., & Bates, P. D. (2014). Regional flood dynamics in a bifurcating mega delta simulated in a global river model. *Geophysical Research Letters*, *41*, 3127–3135. https://doi.org/10.1002/2014GL059744

Yuan, T., Lee, H., Jung, H. C., Aierken, A., Beighley, E., Alsdorf, D. E., et al. (2017). Absolute water storages in the Congo River floodplains from integration of InSAR and satellite radar altimetry. *Remote Sensing of Environment*, *201*, 57–72. https://doi.org/10.1016/j.rse.2017.09.003

Zhang, L., Lu, J., Chen, X., Liang, D., Fu, X., Sauvage, S., et al. (2017). Stream flow simulation and verification in ungauged zones by coupling hydrological and hydrodynamic models: A case study of the Poyang Lake ungauged zone. *Hydrology and Earth System Sciences*, *21*(11), 5847–5861. https://doi.org/10.5194/hess-21-5847-2017

Zhao, F., Veldkamp, T. I. E., Frieler, K., Schewe, J., Ostberg, S., Willner, S., et al. (2017). The critical role of the routing scheme in simulating peak river discharge in global hydrological models. *Environmental Research Letters*, *12*(7), 075003. https://doi.org/10.1088/1748-9326/aa7250